Case Studies in Construction Materials 20 (2024) e03346

Contents lists available at ScienceDirect

Case Studies in Construction Materials

journal homepage: www.elsevier.com/locate/cscm

Using construction and demolition waste materials to alleviate the negative effect of pavements on the urban heat island: A laboratory, field, and numerical study

Mohsen Shamsaei *, Alan Carter, Michel Vaillancourt

Department of Construction Engineering, École de Technologie Superieure, 1100 Notre-Dame Street West, Montréal, QC H3C 1K3, Canada

ARTICLE INFO

Keywords:
Urban heat islands
Reflectivity
Chip seal
Construction and demolition waste
Solar energy absorption
CFD simulation

ABSTRACT

In this study, construction and demolition waste (CDW) materials, including waste clay bricks, concrete, and glass, were used as aggregates of chip seal layers to enhance the reflectivity and reduce the temperature of asphalt pavements as an urban heat island (UHI) mitigation policy. UHI is an urban area that has a higher temperature in comparison to its suburbs. As considerable parts of cities are covered with asphalt pavements, their heat absorption and heat release can directly affect the UHI. Four types of chip seal layers, containing CDW aggregates were prepared in this study. The reflectivity and cooling effects of asphalt pavement coated with the developed chip seals were then evaluated with laboratory, field experiments, and computational fluid dynamics (CFD) simulation. Regarding the laboratory methods, UV-Visible-NIR spectrometer reflectance, a trident thermal properties measurement, and solar simulation cooling effect were used. Besides, the albedo and cooling effects of the developed chip seals were evaluated with a pyranometer and thermocouples through a field experiment. The indoor reflectance test showed yellow and red brick chip seals reflected almost 136 % higher than the aged asphalt pavement, followed by concrete chip seals with 80 % higher solar reflectance. Besides, the surface temperatures of yellow brick, red brick, and concrete chip seals were 23 %, 18 %, and 15 % cooler than the hot mix asphalt (HMA) specimens. More importantly, clay brick chip seals had the lowest nighttime heat release, followed by the concrete chip seal. The field test indicated that the albedo of yellow brick was 2 and 6 times higher than the aged and new HMA, causing 17 % and 27 % lower surface temperatures. The numerical models also revealed that using the yellow brick and concrete chip seals decreased the surrounding air temperature at least by 18 % and 14 % respectively. Overall, the numerical modeling, laboratory, and field tests showed similar results, indicating the benefits of using clay bricks and concrete aggregates for chip seal development, which can mitigate the UHI effectively.

1. Introduction

Asphalt pavement is one of the most common types of pavement due to its simple and fast implementation and maintenance. However, this type of pavement can cause some environmental issues. One of these issues is attributed to solar energy absorption. As a result, its temperature can reach up to 70 ℃ during summer days [1]. As a result, it releases the absorbed heat into the environment,

* Corresponding author.
E-mail address: Mohsen.shamsaei.1@ens.etsmtl.ca (M. Shamsaei).

https://doi.org/10.1016/j.cscm.2024.e03346
Received 6 April 2024; Received in revised form 5 May 2024; Accepted 26 May 2024
Available online 29 May 2024

causing a phenomenon called the urban heat island (UHI) [2]. The UHI is an urban area whose temperature is higher than its rural area and surroundings. This temperature difference can be from 5 to 15 ℃ [3]. In general, for a certain urban area in the US, a considerable part of the city (29–39 %) is covered with pavement [4], showing the impact of pavements on the UHI.

The UHI effects can be exacerbated by some factors, including heat emissions caused by humans, reduction of vegetation cover in cities, high heat absorption of construction materials, and dark surfaces of pavements [5]. As a result, residential water consumption, air quality, building energy consumption, and greenhouse gas (GHG) emissions are negatively affected [6]. It was also concluded that compared to rural places near London, the amount of CO_2 emission will be approximately 4.5 % higher for hot urban areas in London by 2050 [7]. Besides, illnesses and deaths related to heat waves are associated with negative UHI effects [8,9]. Hence, it is necessary to find some solution for UHI mitigation.

Among all contributing factors, the dark color of asphalt pavement is reported to be one of the main reasons for this high solar energy absorption, exacerbating the UHI effects [10]. When the asphalt pavement's surface has high temperatures, it has a high energy absorption rate. Thus, some methods should be used to decrease this absorption rate [11]. One recommended way to decrease the solar absorption rate of asphalt pavements is to increase their reflectivity. It was concluded that when the albedo was raised by 0.1, the surface temperature dropped by 2.1 ℃ [12]. Therefore, some approaches are used to increase the reflectivity of asphalt pavements.

Another environmental issue is related to construction and demolition waste (CDW) in the modern world. According to the statistics, China generated a considerable amount of CDW (1704×10^6 tons) due to urbanization in 2018 [13]. Nevertheless, only less than 10 % of this waste is currently recycled in China [14]. The CDW generations for the USA and Europe were approximately 600×10^6 and 372×10^6 tons respectively [13]. This waste generation in Australia was around 27×10^6 tons which was 61 % higher than this amount in 2006 [15]. A considerable amount of CDW (27 % of municipal solid waste) is generated in Canada, discharging mostly into landfills [16]. Overall, more than 10 billion tons of CDW are annually generated in the world [17]. Waste concrete and bricks account for the largest proportions (almost 59 %) of building CDW materials which need practical solutions to recycle them [18]. Although the CDW recycling rates for Canada, the US, and the EU are higher than other countries such as China (below 10 %), the recycling rates of brick and concrete wastes, accounting for the largest proportions (almost 59 %) of building CDW materials, are not high. As a result, these building construction wastes are usually discharged to landfills [18–20]. Some of the waste clay bricks, kept in a landfill in Montreal (Canada), are depicted in Fig. 1.

Asphalt pavement deteriorates due to the climate effects and traffic loads, and repairing and replacing the distressed pavement needs high budgets and can bring about environmental issues. Thus, using preventive or corrective maintenance methods such as chip sealing and microsurfacing is of major significance [21,22]. Chip seals are reported to be one of the most cost-effective types of bituminous surface treatments which can be used as a preventive maintenance method for both asphalt and concrete pavements [23]. Chip seals are comprised of a layer of bitumen emulsion (de-ionized water, 60–70 % asphalt cement, and an emulsifying agent) covered by one or multiple layers of aggregates compacted before the bitumen emulsion setting [24]. As chip seals are applied at the surface of pavements and aggregates are visible, it can be a practical method to increase the reflectivity of pavement using light color-recycled aggregates without making the pavement slippery. The mechanical properties, safety, and performance of chip seals developed with recycled clay bricks, concrete, and glass aggregates were evaluated in a recent study [25]. The reflectivity and cooling effects of these chip seals, which can alleviate the UHI effects, are of great importance.

The main objective of this study is to propose a novel method to mitigate the UHI effects associated with pavements, using chip seals developed from recycled light color aggregates. The sub-objective of this research is to find this UHI mitigation method using CDW materials which can also be beneficial to recycle these waste materials. Unlike the previous UHI mitigation studies in which pigments and coating were applied on the asphalt pavement surface, reducing surface friction and increasing maintenance costs, this study proposes a new approach to increase the surface reflectivity and surface friction of asphalt pavement as well as sealing the surface cracks. For this purpose, 4 different CDW aggregates, including recycled concrete, yellow and red bricks, and glass were used to prepare chip seals and increase the surface reflectivity of the asphalt pavement. In our previously published articles, the mechanical properties, safety, and durability of these chip seals were evaluated and they met the standard requirements [25,26]. In this study, different laboratory and field experiments were used to measure the reflectivity and cooling effects of these chip seals. The laboratory

Fig. 1. Waste clay brick materials (3RMCDQ landfill in Quebec).

part consists of tests with a spectrometer reflectance with ultra-violet (UV), visible, and near-infrared (NIR) wavelength (identified as UV-Visible-NIR in the text), measurement with a trident thermal properties instrument (C-Therm), and infrared solar simulation tests. Besides, the albedo measurement with a pyranometer, surface, and in-depth temperatures were monitored and recorded with an infrared camera and thermocouples through a field test. In addition to the field and laboratory tests, the ANSYS Fluent software package was used to carry out computational fluid dynamics (CFD) simulation for heat transfer inside the pavement and heat exchange with the environment. Finally, the effects of using these CDW materials on the UHI were examined and discussed. The outline of this study is demonstrated in Fig. 2.

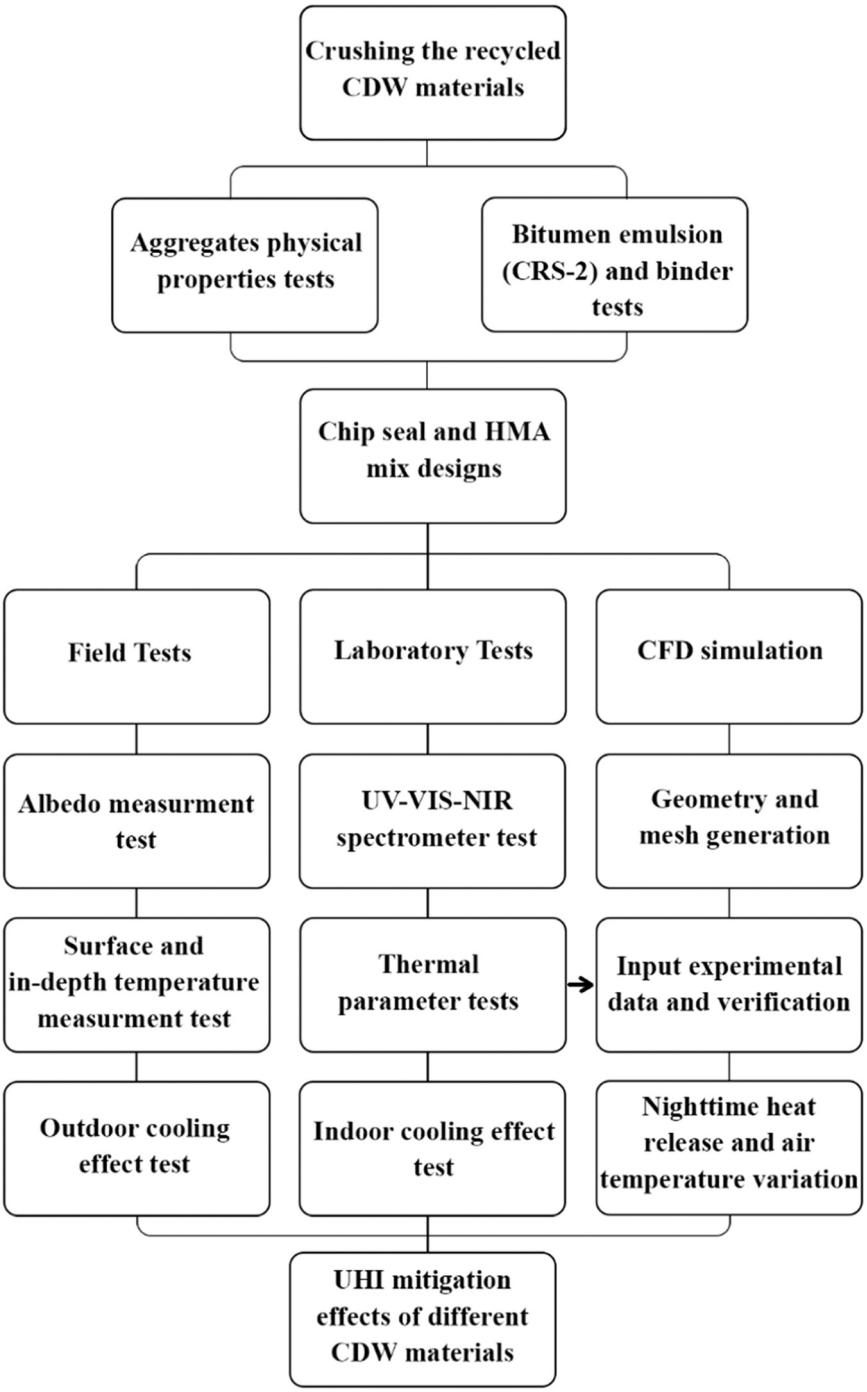

Fig. 2. The research outlines.

2. Literature Review

Different methods have been used to combat the negative UHI effects, stemming from the dark surface of pavements. Almost all of these studies were conducted based on three main principles, including increasing the pavements' reflectivity, cooling down the pavement with water (evaporative pavements), and changing the pavements' materials to alter the heat transfer rate of pavements [2]. Regarding reflective pavements, the main principle for them is to increase the pavement's albedo, altering the pavement's thermal inertia [27]. This is a nondimensional parameter that shows the ratio of the reflected radiation. New asphalt pavement has an albedo of 0.05, meaning 95 % of the solar radiation is absorbed and only 5 % of it is reflected. [28].

The most common method for increasing the asphalt pavement albedo is using pigments and heat-reflective coatings. In a recent study, ten different coatings were used to increase pavement reflectivity. The test results showed that the pavements coated with these pigments could have visible light reflectance and near-infrared reflectance up to 60 % and 95 %, respectively [29]. Nanocomposite reflective coatings were also used for the same purpose and the results revealed that the pavement's heat radiation and convection were reduced by 66 % and 50 %, respectively. This means that these materials could mitigate the UHI and increase the human body's thermal comfort [30]. In another study, the effect of coating concrete and asphalt pavements with heat-reflective pigments on the air temperature was examined in different climate conditions. The results indicated that the air temperature surrounding the concrete and asphalt pavements coated with these pigments was 1 ℃ and 5 ℃ cooler, respectively [31]. Another heat-reflective coating was also developed with epoxy resin emulsion. Different functional fillers, including titanium oxide, diatomite, substrate, silicon dioxide, and fumed silica were added to the surface. The results revealed that the usage percentage of filler should be less than 30 % (by weight) of the coating, and the 2 % iron oxide for making light gray coating had the best cooling effect and visual comfort. When 0.8 kg/m^2 of this coating was placed on the pavement, the surface temperature decreased by almost 10.4 ℃ [32].

Although using these kinds of pigments and coating can decrease the pavements' temperatures and mitigate the UHI, they can negatively affect the drivers' vision and skid resistance. To solve glare issues, some pigments, which were not white, with near-infrared reflection were used [33]. Despite these pigments looking dark, they could increase the asphalt pavement albedo from 0.4 to 0.7 [34]. Regarding the skid resistance reduction by using these pigments, ceramic particles, and special sand were used which increased the skid resistance by 50 % [35]. Besides, the performance of these coatings deteriorated over time under natural weathering conditions. Thus, anti-aging additives were added to these pigments. The results showed that the reflectance percentage change was less than 10 % for white coatings and less than 5 % for colorful coatings [36]. However, the durability of fillers and particles for increasing the skid resistance of pavements containing these coatings has been questionable, and some of these pigments have harmful chemical compositions that are not environmentally friendly. More importantly, considering all requirements for pavements coated with these pigments with sufficient skid resistance and durability can increase pavement construction and maintenance costs.

Researchers have also tried to recycle CDW and other wastes as pavement materials [37–41]. In a study, waste clay, ceramic, and mortar were used as concrete paving aggregates. The experimental tests revealed that these materials increased the concrete water absorption and apparent porosity, reducing the splitting tensile and compressive strengths. However, using these materials up to 50 % met the minimum strength of concrete paving [42]. In hot mix asphalt (HMA), natural aggregates were replaced with recycled concrete up to 30 %. The results of stiffness, permanent deformation, fatigue, and moisture sensitivity revealed that this material enhanced the HMA stiffness, moisture susceptibility, and rutting resistance. However, HMA containing recycled concrete showed a lower fatigue life, affecting the load transfer efficiency of asphalt pavement significantly [43–45]. The recycled concrete powder was also used as a filler for cold mix asphalt (CMA). The results showed that fatigue life, moisture sensitivity, tensile strength, abrasion loss, rutting resistance, and stability of CMA were improved after adding 1–3 % (by weight of the mixture) of concrete powder [46]. The CDW materials, including recycled clay masonry and concrete, were also used as base course aggregates up to 100 %. The numerical modeling showed that the rutting resistance and fatigue cracking of asphalt pavement constructed on the developed base course were improved [47]. The recycled glass was also used both as the granular base course and asphalt mixture materials. The results showed that using recycled glass up to 25 % and 10 % (by weight) had marginal effects on the mechanical properties of the base course layer and HMA respectively [48,49]. Consequently, despite a myriad of positive effects of CDW on pavement performance, these materials have not been used to develop chip seals for pavements.

A numerical study was conducted using ENVI-met software to assess the air temperature of a parking area coated with light concrete, stone, bricks, grass, and wood instead of asphalt pavement. The result showed that the existing asphalt pavement caused the highest air temperature [50]. Therefore, using these kinds of materials as exposed materials on the surface of pavements, such as chip seals, can reduce the air temperature and mitigate the UHI effects. Besides, different waste materials have been used to develop chip seals in recent years. For instance, the natural aggregates of chip seal were replaced with crumb rubber in a study. The skid resistance and aggregate embedment were evaluated, and the results showed that these waste materials had sufficient embedment and skid resistance [51]. In another study, the natural aggregates of chip seals were replaced with reclaimed asphalt pavement (RAP). The chip seal mechanical test results revealed that RAP materials could meet the chip seal mix design standards [52]. Considering the skid resistance, chemical compositions, and durability issues of pigments used to increase the reflectivity of pavements, using CDW materials as chip seal aggregates can not only be a practical method to recycle these materials, but it may be a suitable approach for raising the pavement surface reflectivity [25]. As the asphalt mixture layer plays the most important part in temperature distribution and heat transfer of asphalt pavement structure, modification of the surface reflectivity and thermal properties using materials with different properties can affect heat absorption and heat release dramatically. Considering the thermal properties of asphalt pavement, prediction models can be developed to estimate the pavement temperature containing materials with different thermal properties [53,54].

3. Materials and Methods

3.1. Materials

Aggregates and bitumen emulsion form the chip seal. In this study, 4 different recycled materials, including concrete, yellow brick, red brick, and glass, were used as chip seals' aggregates. These materials were provided from two recycling sites in Canada (The 3RMCDQ and the RITMRG in Quebec). Firstly, the recycled aggregates were crushed with a laboratory crusher. They were then sieved to have certain ranges of aggregates. The aggregate sizes are depicted in Fig. 3. Only one range coarse aggregate (between 5 and 10 mm) was chosen for both concrete and brick aggregates. The glass aggregates' sizes were smaller (between 2.36 mm and 6.3 mm). The reason why this aggregate was smaller was to avoid flaky aggregates and tire wear. The physical properties of these aggregates are evaluated and reported in Table 1.

The bitumen emulsion used in this study was Cationic Rapid Setting type 2 (CRS-2). This is one of the most common bitumen emulsions for chip seal preparations, whose properties are mentioned in Table 2. The bitumen emulsion provider recommended using it at a certain temperature which was between 60 and 85 ℃. Thus, the bitumen emulsion temperature was 65 ℃ for all specimens. The water breaks out of bitumen emulsion for specimen curing was measured. The bitumen emulsion was placed at 35 ℃ and its weight loss was recorded for 48 hours. The weight loss trend is illustrated in Fig. 4. According to this diagram, because of the water breakout, its weight was reduced by 25 % and 30 % after 6 and 24 hours respectively.

3.2. Chip Seal Mix Design

There are some common methods used to design chip seals in North America, including Kearby, McLeod, modified Kearby, and modified McLeod approaches [68–70]. All these methods have the same aim which is the calculation of aggregates and binder application rates to have 50–80 % of median aggregate size embedment. In this study, the McLeod method was used in accordance with the Minnesota seal coat handbook [71]. According to this method, the aggregate application rate depends on physical properties, including gradation, aggregate shapes, and specific gravity. The binder application rate relies on aggregates' shape and absorption, pavement surface conditions, traffic volume, and the binder's asphalt content. The aggregate application rate is calculated with Eq. 1.

$$C = [1 - 0.4V] \times H \times G \times E \tag{1}$$

Where C is the aggregate application rate (kg.m^{-2}), V is void in the loose mix, H is the average least dimension (mm), G is the bulk specific gravity, and E is the wastage factor for traffic whip-off, which indicates the number of aggregates that will get thrown to roadway sides during chip seal curing under traffic loads. The wastage factor is assumed 5 and 10 percent for low-volume and high-

Fig. 3. The recycled aggregates used in this.

Table 1
The physical properties of aggregates.

Physical Properties	Standard	Concrete	Yellow brick	Red brick	Glass
Density (kg/m^3)	[55]	2370	1933	1907	2491
Loose unit weight (kg/m^3)	[56]	1514	1117	1122	1486
Water absorption (%)	[55]	4.71	13.56	14.13	0.16
Los Angeles (%)	[57]	23.5	39.5	41.5	44.5
Flakiness index (%)	[58]	14	19	21	30
Median particle size (mm)	[59]	6.50	6.70	6.80	4.70

Table 2
The properties of bitumen emulsion.

Tests	Unit	Test method	Result For CRS-2	Specifications	
				Min	Max
Residue by distillation (weight)	%	[60]	69.1	65	-
Oil Distillate, (volume)	%	[60]	0.32	-	3
Demulsibility	%	[61]	85.1	40	-
Saybolt Furol viscosity at 50 °C	Sec	[62]	223.4	100	400
Settlement and storage stability, 1 day	%	[63]	0.312		Max 1
Penetration, 25 °C, 100 g., 5 s.	0/1 mm	[64]	153.3	100	250
Particle Charge	-	[65]	Positive	-	-
Ductility, 4°C, 5 cm/min	cms	[66]	75.1	40	-
Solubility in TCE	%	[67]	99.51	98.5	-

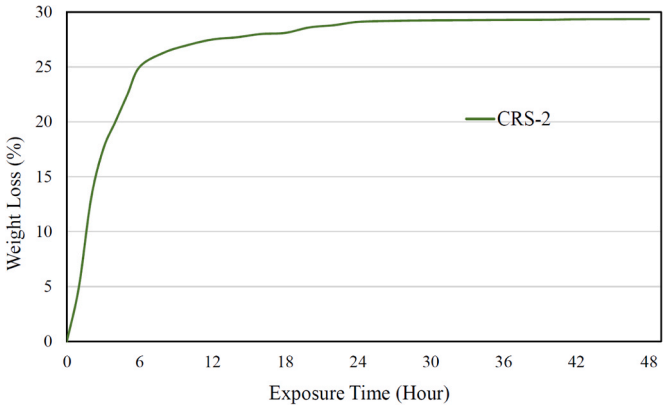

Fig. 4. The bitumen emulsion weight loss due to water breakout.

volume traffic roads, respectively. The application rates of aggregates were calculated with Eq. 1 and experimental tests. Thus, the application rates of glass, concrete, yellow brick, and red brick aggregates were 4.85 kg/m^2, 7.88 kg/m^2, 6.11 kg/m^2, and 6.02 kg/m^2 respectively. The binder application rate is also calculated with Eq. 2.

$$B = \frac{[0.4 \times H \times T \times V] + S + A}{R} \quad (2)$$

Where B is the binder application rate (L/m^2), H is the average least dimension (mm), T is the traffic factor, V is the voids is loose aggregate, S is the surface condition factor (L/m^2), A is the aggregate absorption factor (L/m^2) and R is the residual asphalt content of binder. Considering the experimental tests and Eq. 2, The emulsion rates for glass, concrete, yellow brick, and red brick chip seals were 1.44 L/m^2, 1.50 L/m^2, 1.88 L/m^2, and 1.90 L/m^2. Special molds were made with the average least dimension (ALD) height, and the relevant aggregates and bitumen emulsion were placed inside them and compacted to check the calculated application rates. The results showed that the mentioned application range exactly filled the molds, and due to almost 30 % water loss (Fig. 4), the aggregate embedment was almost 70 %.

3.3. Asphalt Mixture Design

The laboratory asphalt mixture specimens were prepared based on the Quebec standard [72]. The nominal aggregate size was 10 mm (ESG-10 asphalt mixture), and PG 58–28 asphalt binder, modified with anti-stripping agents, was used to prepare the dense

graded hot mix asphalt. The asphalt mixture and binder characteristics and aggregate gradation are depicted in Table 3 and Fig. 5, respectively. Based on the Quebec standard, the mixing temperature was 150 ℃, and the mixture was compacted using a gyratory compactor at 135 ℃ to prepare cylindrical specimens with 150 mm in diameter and 150 mm in height.

3.4. The Laboratory and Field Tests

3.4.1. Ultraviolet (UV)-Visible-Near Infrared (NIR) Spectrometer Test

A UV-Visible-NIR spectrometer (Perkin Elmer- Lambda 750) was used to measure the reflectance and absorption of chip seals. This device can measure the absorbance and reflectance of wavelengths ranging from 175 nm to 3000 nm. The range of temperature can also be between 0 ℃ and 100 ℃ during the test. Although, the maximum dimension of solid samples for this device is 100×100 mm, the dimension of chip seal samples was 50×50 mm to have more accurate results and fewer errors. Consequently, the relevant amounts of aggregates and bitumen emulsion were used to prepare the specimens for this test. Therefore, approximately 12 g, 20 g, 15 g, and 16 g of glass, concrete, yellow brick, and red brick aggregates were placed on 4 g, 4 g, 5 g, and 5 g bitumen emulsion respectively, followed by compaction with a 1 kg roller compactor. The specimens were then cured at 35 ℃ for 48 hours, followed by 48 hours of curing at the ambient temperature to break out the bitumen emulsion water. Two other specimens were cored and cut from new HMA and an aged HMA (after 3 years) for this experiment. The absorbance and reflectance of each specimen were measured five times while the specimens were rotated, their positions were changed before each measurement, and their averages were finally calculated. The Lambda 750 spectrometer and the specimens for this test are depicted in Fig. 6.

3.4.2. Thermal Properties Measurement

As these waste materials are exposed to direct solar radiation and they form the top surface of the pavement, their thermal properties are of great importance. A trident thermal conductivity instrument (C-Therm) was then used to measure the heat transfer of these materials separately, which works based on the ASTM Standard [73]. This device has different sensors, all of which work based on the transient heat transfer method. In this study, the modified transient plane source (MTPS) sensor was used for thermal conductivity and thermal effusivity measurements, which is recommended for solid materials. The minimum diameter of the solid sample for this sensor is 18 mm, and the sample should have a flat surface. Since having this requirement for prepared chip seals was not possible due to the aggregate sizes (5–10 mm with rough surfaces), this test was conducted on the aggregates before crushing. Indeed, these 4 waste materials and new and aged asphalt pavement were cut (50×50) to have smooth and flat surfaces for thermal property measurements. To have sufficient contact between the materials and the MTPS sensor, a special paste (provided by the C-Therm supplier) was then used to fill the voids, and each specimen was loaded with a 500 g weight. The C-Therm device had some reference samples on which this thermal paste was used, and the measured thermal properties remained unchanged before and after using this agent. Finally, the thermal conductivity of each specimen was measured 5 times on different spots of each specimen. The C-Therm device and specimens are demonstrated in Fig. 7.

3.4.3. The Indoor Solar Simulation Test

An experimental setup was developed to simulate an indoor test for evaluating the one-directional heat transfer in the asphalt mixtures coated with chip seals. A 175 W tungsten iodide (infrared) lamp with a wavelength, ranging from 300 nm to 3000 nm, was used to simulate the solar radiation for specimens. A transparent pipe with the same diameters of asphalt mixture (150 mm) was also used to minimize the airflow and ventilation at the top of the specimens. The pipe was also used to concentrate the heat and reach a certain temperature for the control HMA specimen. The highest possible surface temperature of asphalt pavement in Canada was the target of the test since the UHI effects are more important during hot weather. Therefore, considering the highest pavement temperatures in Canada [74], the height of the lamp was determined (85 cm) with trials and errors. In the first step, the control asphalt mixtures were placed in the setup shown in Fig. 8, and the infrared lamp was lit for 15 hours until the asphalt mixture surface temperature reached 63 ℃. The lamp was then turned off for 9 hours to record the temperatures and the reverse heat transfer from the specimens to their surroundings. In each sample, 7 thermocouples were placed and held with bitumen depicted in Fig. 8. These thermocouples and an air temperature sensor were connected to a data logger to record the temperatures during the receiving and releasing heat procedures. The surface temperatures of specimens were also monitored and recorded with an infrared camera during the test. All specimens were also surrounded with liquid foams to minimize the heat transfer from their sides and bottom with their surroundings.

Table 3
Asphalt mixture and asphalt binder characteristics.

PG 58–28 asphalt binder properties	Values	ESG-10 asphalt mixture Properties	Values
Density at 25 ℃ (g/cm^3)	1.025	G_{mm} (g/cm^3)	2.538
Viscosity at 135 °C (Pa·s)	0.247	Binder (%) by weight	5.45
Viscosity at 165 °C (Pa·s)	0.075	Absorbed binder (%) by volume	1.02
G*/sin δ at 58 ℃ for virgin binder (kPa)	1.254	Effective binder (%) by volume	12.2

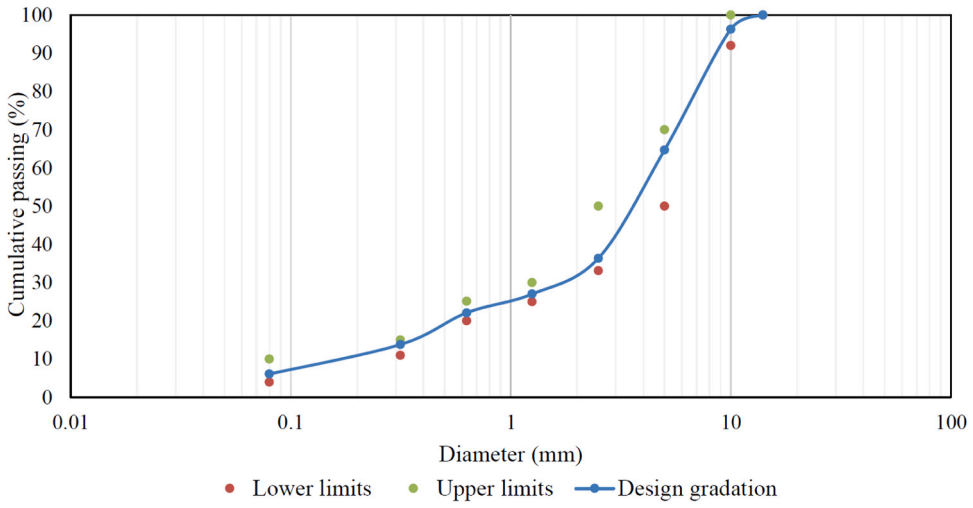

Fig. 5. The aggregate gradation of asphalt mixture specimens.

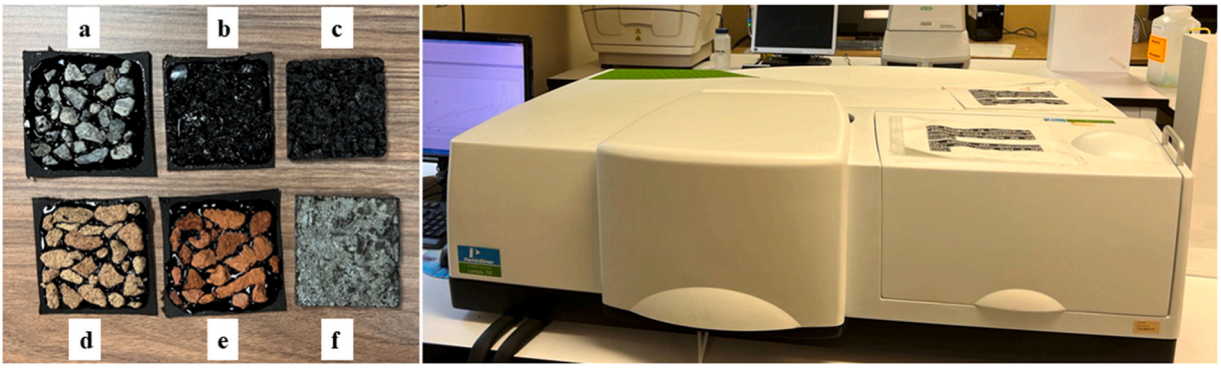

Fig. 6. Specimens for the reflectivity test (left): (a) concrete, (b) glass, (c) new HMA, (d) yellow brick, (e) red brick, (f) aged HMA, and the Lambda 750 spectrometer device (right).

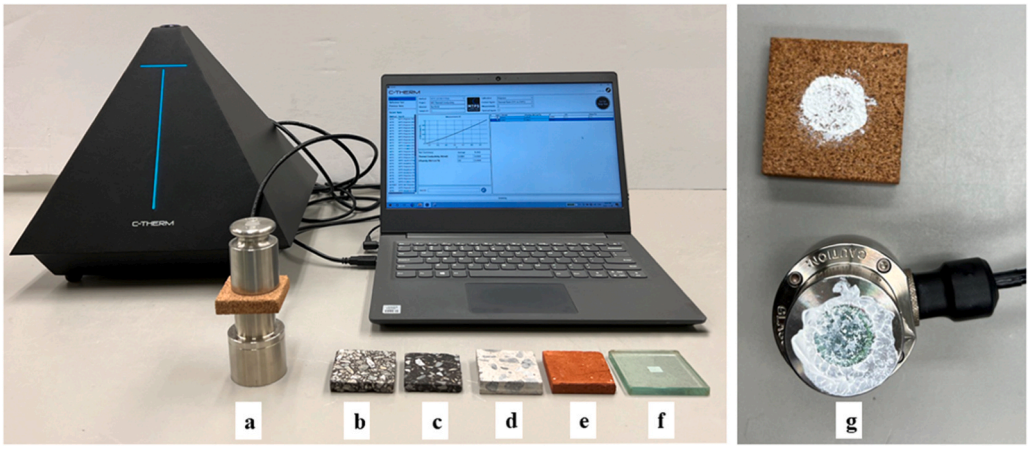

Fig. 7. The thermal conductivity measurement of materials: (a) yellow brick, (b) aged HMA, (c) new HMA, (d) concrete, (e) red brick, and (g) the MTPS sensor with the contact paste.

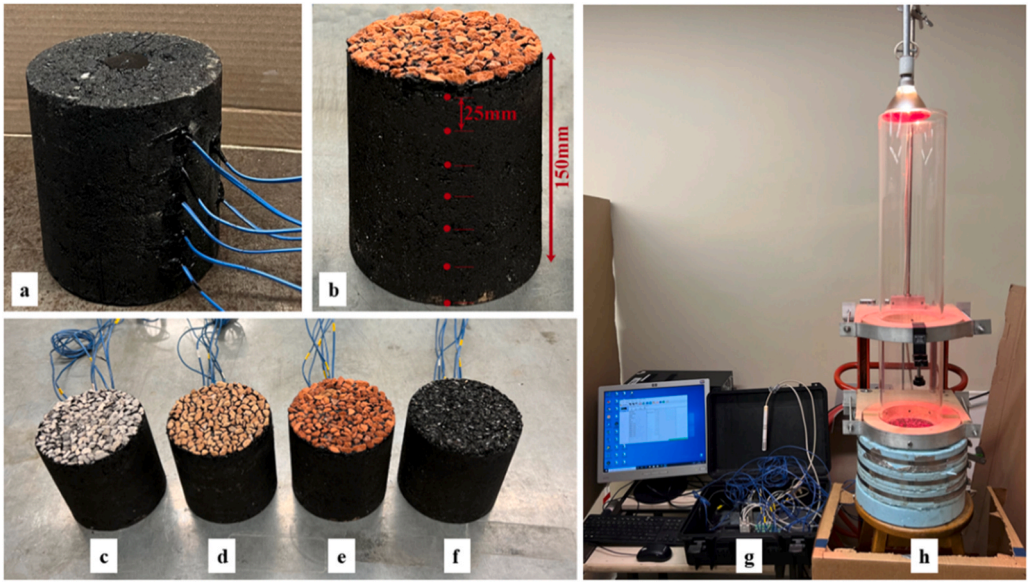

Fig. 8. The solar simulation test: (a) thermocouple placement, (b) thermocouples' locations, (c) concrete, (d) yellow brick, (e) red brick, (f) glass chip seals, (g) the data logger and computer, (h) the insulated sample and lamp.

3.5. The Field Test for Solar Reflection

The solar spectrum has different wavelengths, ranging from 200 nm to 2500 nm (approximately 96.3 % of the total irradiance) [2]. Although tungsten lamps are reported as one of the most practical methods to simulate solar energy for pavements [75], their color

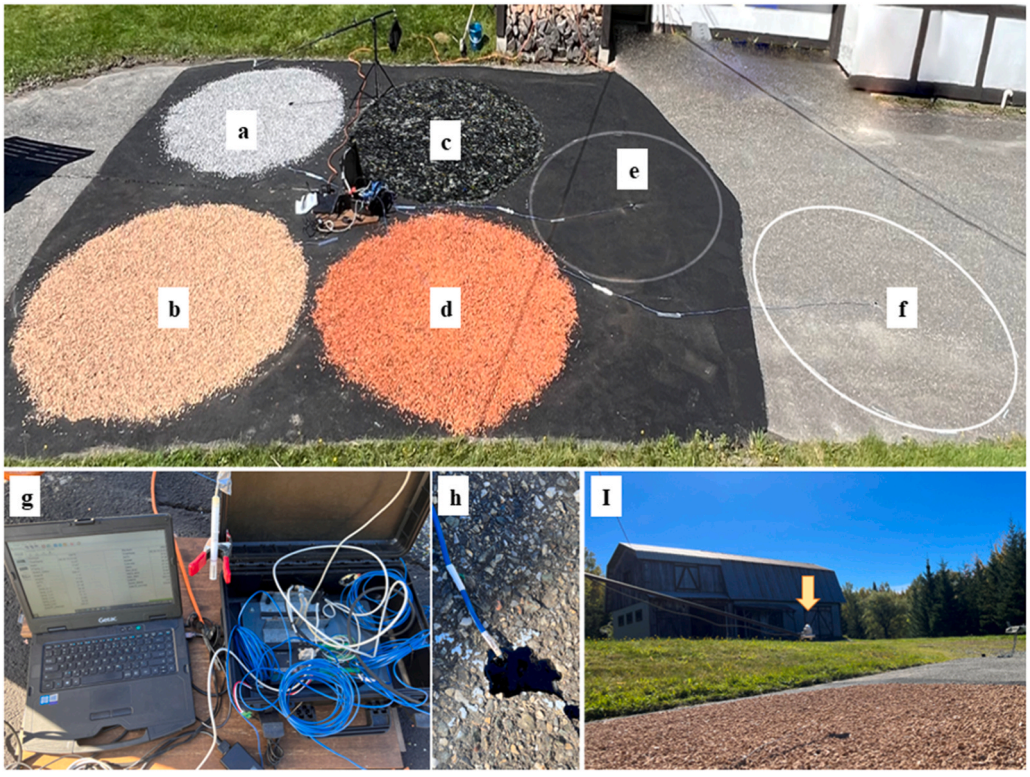

Fig. 9. The field reflection test details: (a) concrete, (b) yellow brick, (c) glass, (d) red brick chip seals, (e) new HMA, (f) aged HMA, (g) the data logger, (h) the thermocouple placement, (I) the pyranometer and cloudless sky.

temperatures are 3200k. However, the solar spectrum brightness temperatures range from 5600k to 6000k. Thus, the shortwave visible output and low UV can differentiate between solar radiation and the simulation approach [76]. Considering all these factors, the albedo and cooling effects of chip seals were evaluated with an outdoor test. Therefore, 4 different circular asphalt pavement areas with diameters of 4 m were covered with bitumen emulsion and waste aggregates, including yellow and red bricks, concrete, and glass. Moreover, the albedo and temperatures of two other circular areas, including newly constructed and aged asphalt pavements (with the same diameters) were investigated. The albedo measurement test was carried out based on ATSM E1918 (2021) [77]. According to this standard, the albedo should be measured in a cloudless weather condition when the sun's angle to the normal of the pavement surface is lower than 45°. Indeed, if the surface is low-sloped or horizontal, this test should be done between 9 a.m. and 3 p.m. local time. In winter, however, as the solar incidence has a lower angle, the test should be performed between 10 a.m. and 2 p.m. local standard time. As this test was conducted on 30/09/2022 in Orford (Quebec, Canada) which was cloudless and sunny, the reflection was measured three times for each area from 11 a.m. to 2 p.m. local time. According to a previous study, the air temperature and wind speed do not affect the albedo [78]. The reflection values should be constant for at least 10 s for each reading, and three pairs of readings were recorded for incoming and reflected solar incidence in 2 minutes. The distance of the albedo meter was 500 mm from the surface and when the incoming radiation was recorded, it was flipped down to measure the reflected radiation for each area. Besides, 6 different thermocouples were placed in the center of each area at 25 mm depth to record the asphalt pavement temperatures. All these thermocouples, the pyranometer, and an air temperature sensor were connected to a data logger which transferred all data to a computer. Moreover, the surface temperature was also monitored and recorded with an infrared camera. The data logger and air temperature sensor were hidden from the sun to minimize the error during the test. The field test section and its details are depicted in Fig. 9.

3.6. The Computational Fluid Dynamics (CFD) Simulation

The heat transfer between solid and gas should be evaluated with finite element software which can analyze the behavior of the flow of gases and fluids. Compared to other software used for microclimate research, ANSYS Fluent works based on CFD algorithms which is suitable for modeling fluid dynamics, thermal reactions, heat transfer through Reynolds-averaged Navier Stokes (RANS) equations, and k-epsilon (k-ε) turbulence model [79]. As the UHI stems from the released heat from the pavement to the air, the heat transfer from the pavement to the air should be assessed with fluid dynamic equations. Hence, the ANSYS Fluent software package was utilized to evaluate the heat transfer inside the asphalt mixture and the heat exchange with the environment. Different models were developed for both asphalt mixture and chip seal samples to examine not only the heat transfer rate for each sample but also the air temperature reduction after using chip seals. Therefore, the experimental data for the chip seal which provided the cooler surface and control HMA was used for this simulation. Thus, all types of heat transfer, including radiation, convection, and conduction were involved in the simulation, and all required thermal parameters were obtained from the indoor solar simulation test.

3.6.1. Geometry and Mesh Generation

Two different models were developed with sufficient widths and lengths to simulate the real field situation. Indeed, the dimensions of the control HMA and chip seal models were 8 m ×10 m × 0.15 m and 8 m ×10 m × 0.16 m, respectively. Besides, a certain volume of air at the top of the pavements (10 m height) was included in the models. The pavement meshes were structured and the air meshes were both structured and unstructured. The first layer of air elements' size at the top of the pavement surface was 1 mm to have a suitable accuracy. The air element sizes then grew in a structured shape with a 1.2 growth rate for the next 20 layers. The unstructured elements were also used for the upper layers of air in the models. Overall, each model consisted of 2,071,300 elements. The details of

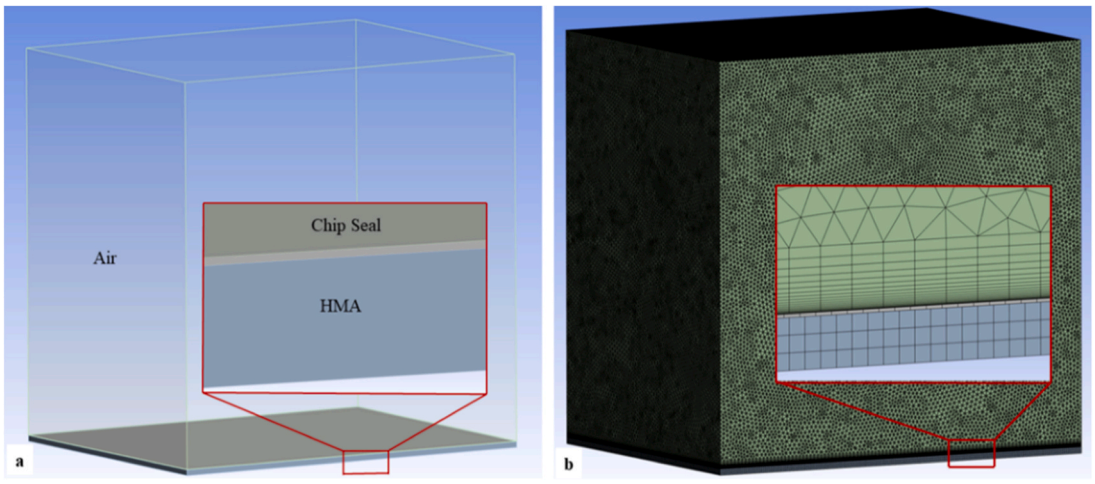

Fig. 10. The chip seal model; (a) Geometry and (b) meshing details.

geometry and meshes for the chip seal model are demonstrated in Fig. 10. The HMA models had similar geometry and meshes, except for the chip seal layer.

3.6.2. The Simulation Conditions

The transient heat transfer was used for this simulation. The standard k-ϵ model was employed to have air turbulence effects at the top of the pavement. The boundary conditions comprised the necessary temperatures, interface properties, and wind details. The air inlet and outlet velocity, pressure, and temperature were also defined based on the obtained experimental results. The left, right, and top sides of the model were assumed to be symmetric. These sides and the bottom of the pavement were also assumed to be adiabatic, preventing heat exchange with the model's surroundings. The inflow wind boundary conditions were applied with an expression to have leading wind at 10 m height with 2 $m.s^{-1}$ speed, which represents summer. Besides, the interface of chip seal and asphalt mix temperature and contact specifications, and surface and in-depth temperatures, obtained from the laboratory tests were involved in the model's boundary conditions. The details of wind velocity and the model's airflow are illustrated in Fig. 11. In this figure, the wind speed equation is depicted, where U ($m.s^{-1}$) is the wind speed and Y is the height (m). The inlet and outlet airflow over the pavement is shown in Fig. 11 (b).

3.6.3. Input Thermal Parameters

The transient heat conduction, altering the temperature during the time with other thermal parameters, was performed based on Eq. 3.

$$\Delta T = \frac{1}{\alpha} \cdot \frac{\partial T}{\partial t} \tag{3}$$

Where ΔT represents the temperature difference, α is the thermal diffusivity ($m^2.s^{-1}$), and t is the time (s). The other heat transfer mode, convection, was performed based on Newton's law to simulate the heat transfer between the asphalt mix surface and surrounding air, shown in Eq. 4.

$$Q_{convection} = h(T_S - T_{air}) \tag{4}$$

Where T_S represents the surface temperature (K), T_{air} is the air temperature (K), and h is the convective exchange coefficient ($W.m^{-2}.K^{-1}$). The radiation heat transfer was also performed in the simulation process, based on Eq. 5.

$$Q_{Radation} = \varepsilon\sigma(T_{sur}^4 - T_{air}^4) \tag{5}$$

Where T_{sur} represents the pavement surface temperature (K), T_{air} indicates the ambient air temperature (K), ε is the emissivity of the surface, and σ is the Stefan–Boltzmann constant (5.67×10^{-8} $W.m^{-2}.K^{-4}$).

4. Results and Discussion

4.1. The Spectrometer Reflectance Radiations

Each object generally shows three different responses to incident energies, including absorbing, reflecting, and transmitting. Eq. 6 shows the relationship between these parameters[80].

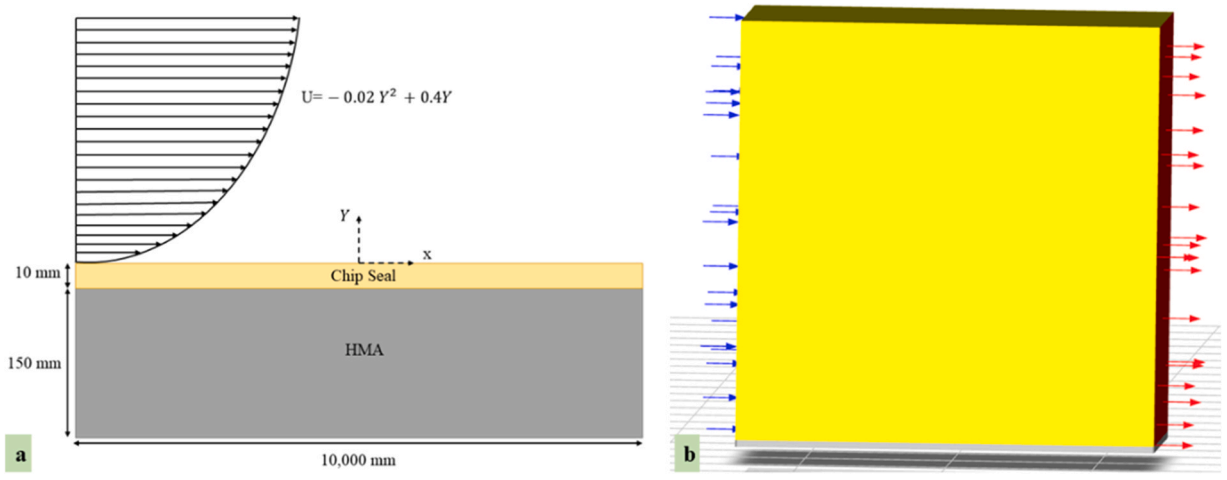

Fig. 11. (a) The wind velocity details and (b) the model's inlet and outlet airflow.

$$\rho + \varepsilon + \tau = 1 \tag{6}$$

Where ρ is the reflectance rate, ε is the absorption, and τ is the transmittance. As asphalt pavement and chip seals are not transparent, τ is equal to zero [80]. Accordingly, higher reflectivity and lower absorption are the main goals to reduce the surface temperature. Considering the solar spectrum, the irradiance with lower than 300 nm wavelengths is mostly absorbed by O_3, and approximately half of the solar irradiance energy (43 %) is in the Visible (wavelengths between 400 and 780 nm) and almost 52 % of its energy is in the near-infrared (NIR) (wavelengths from 800 to 2500 nm) region, demonstrated in Fig. 12 [81,82]. Direct normal irradiance (DNI) is the received radiation at the Earth's surface perpendicular to the Sun, and this irradiance excludes diffuse solar radiation (radiation that is reflected or scattered by atmospheric components).

The results of reflectance for different wavelengths ranging from 300 nm to 2000 nm, obtained from the UV-Visible-NIR spectrometer, are also illustrated in Fig. 13. As can be seen, the chip seal made from yellow bricks had the highest reflectance for all wavelengths. Red brick and concrete chip seals' reflection was ranked second and third, followed by aged HMA, glass chip seal, and new HMA. The combinations of reflection data and the solar spectrum were analyzed to have a better comparison for each region. As a result, the reflectance of different chip seals, aged, and new HMA for solar spectrum (Fig. 13) for each region was calculated with Eq. 7, which is obtained from an ASTM standard [81].

$$R_s = \frac{\int_{\lambda_2}^{\lambda_1} R(\lambda)E(\lambda)d\lambda}{\int_{\lambda_2}^{\lambda_1} E(\lambda)d\lambda} \tag{7}$$

Where R_s is the solar reflectance of chip seals, aged and new HMA (%), $R(\lambda)$ is the measured spectral data from samples and $E(\lambda)$ is the solar spectral irradiance. Thus, the solar reflectance of chip seals and HMA, categorized for each region, is depicted in Table 4. As can be seen, the UV reflectivity of all chip seals, aged and new HMA is less than 6 % percent and they have marginal differences. The yellow chip seal and new HMA had the highest and lowest reflection in the UV region, 5.33 %, and 3.23 %, respectively. Aged HMA and other chip seals ranged from 4.07 % to 5.02 %. Because the UV reflection of construction materials is low due to their surface texture and chemical compositions which were also observed in previous studies [83,84]. Similarly, the same trend was observed for the visible (VIS) region whose reflectance is much more significant than UV regions since it accounts for almost 43 % of solar light, except for the glass chip seal [82]. Indeed, the yellow brick chip seal reflected around 22.58 % of solar radiations in this region, followed by red brick and chip seals, 16.15 % and 14.19 %, respectively. Although the glass chip seal had a good UV reflection, this chip seal and new HMA, however, reflected 32 % and 55 % less than Aged HMA in this region. These reflection percentages are attributed materials' colors. Therefore, as clay brick and concrete have lighter colors, they could reflect more visible light, especially near their colors' wavelengths. These results were comparable to other previous studies in which different colors of coatings were used to change the reflectivity of asphalt pavements and surfaces with coatings and measured the reflection of construction materials [84–87]. Lastly, although the NIR reflection (52 % of total solar energy is in this region) of all specimens had a downward trend, the overall NIR reflection of them was more than the VIS region. Similarly, the yellow brick chip seal also reflected the highest NIR radiation, 26.45 %. The NIR reflection orders of other chip seals were similar to the VIS region, and the glass chip seal and new HMA reflected the least NIR radiations,

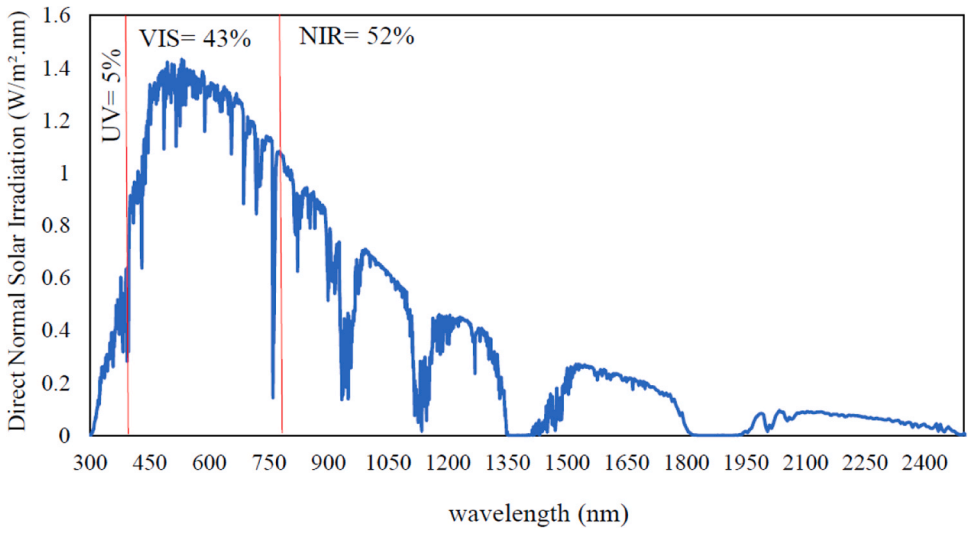

Fig. 12. The solar spectrum energy (direct normal irradiance) [81].

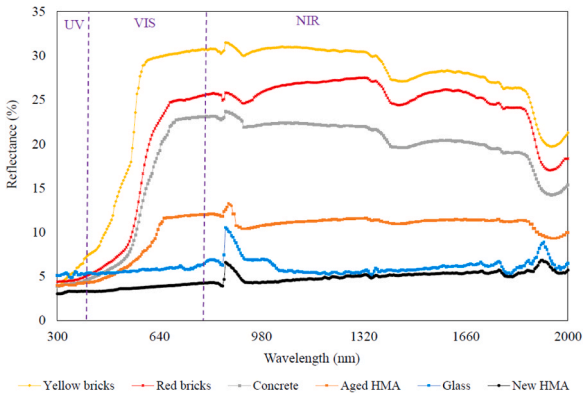

Fig. 13. The spectral reflectance of different chip seals, aged and new HMA.

Table 4
The solar reflectance of different chip seals, aged and new HMA.

Type of surface	Reflectance (%)			
	UV	VIS	NIR	Total (based on wavelengths)
Yellow brick chip seal	5.33	22.58	26.45	24.36
Red brick chip seal	4.57	16.15	23.36	20.61
Concrete chip seal	4.20	14.19	19.20	17.18
Glass chip seal	5.20	5.71	5.75	5.71
Aged HMA	4.07	8.38	10.36	9.54
New HMA	3.23	3.76	4.70	4.40

5.75 %, and 4.70 % respectively. These results are attributed to the chemical composition, molecular structure, surface roughness, and color of chip seals' aggregates, and the results were comparable to previous studies related to increasing the NIR reflection of coatings [88–90]. Considering the total reflections, clay bricks, and concrete chip seals reflected much more solar radiation in comparison to the aged HMA, contributing to the cooler pavement surface and mitigation of the UHI effects substantially.

4.2. Thermal Properties of Chip Seal Aggregates

The average thermal effusivity and thermal conductivity of CDW materials, aged and new HMA, are reported in Table 5. Thermal effusivity indicates the surface material's ability for heat exchange with its immediate surroundings [91]. Accordingly, as aggregates form the surface of chip seals with direct contact with the environment, the thermal effusivity of chip aggregates plays an important role in UHI mitigation since it can either transfer heat to the environment rapidly or hinder this heat transfer. Considering Table 5, yellow and red bricks had the lowest thermal effusivity, 1270.38 and 1381 W. $s^{1/2}$. m^{-2}. K^{-1}, respectively. It means that after receiving the solar energy, clay brick aggregates have the lowest heat exchange with the environment, which can alleviate the UHI effects. This lower thermal effusivity can be associated with their porous textures and lower density, decreasing the effusivity due to air existence and fewer atoms for transferring heat [92]. Glass aggregates had a little higher thermal effusivity (1472.55 W. $s^{1/2}$. m^{-2}. K^{-1}) emitting less heat to their surroundings in comparison to HMA and concrete aggregates. Aged, new HMA and concrete aggregates had the highest thermal diffusivity, exchanging more heat to the environment after receiving solar energy. Therefore, compared to yellow bricks which had the lowest thermal effusivity, the thermal effusivity of aged, new HMA, and concrete was 48 %, 43 %, and 70 %

Table 5
Thermal properties of CDW materials and HMA.

Aggregates & mixtures	Thermal conductivity (obtained from experiments)			Thermal effusivity (obtained from experiments)			Specific heat capacity (J. kg^{-1}. K^{-1}, calculated)	Thermal diffusivity ($mm^2.s^{-1}$, calculated)
	Avg values (W. m^{-1}. K^{-1})	Standard deviation (SD)	Coefficient of variation (CV %)	Avg values (W. $s^{1/2}$. m^{-2}. K^{-1})	Standard deviation (SD)	Coefficient of variation (CV %)		
Yellow brick	0.95	0.01	1.13	1270.38	9.40	0.74	876.84	0.56
Red brick	1.03	0.02	2.13	1381	12.87	0.93	967.61	0.56
Concrete	2.45	0.05	1.90	2162.05	24.33	1.13	806.46	1.29
Glass	1.19	0.00	0.18	1472.55	1.77	0.12	729.74	0.66
Aged HMA	1.91	0.02	1.00	1875.97	10.42	0.56	808.48	1.04
New HMA	1.65	0.02	1.26	1815.22	14.67	0.81	872.97	0.82

higher. The reason is attributed to the different structure and chemical composition of these materials. Furthermore, compared to concrete which is a crystalline solid, glass is a non-crystalline solid with a disordered and random molecular structure [93,94]. Thus, the thermal effusivity of glass is lower.

$$e = (k.\rho.C_p)^{\frac{1}{2}} \tag{8}$$

In addition to thermal diffusivity, another important measured parameter was thermal conductivity. Regarding Table 5, the thermal conductivity of materials was similar to the thermal effusivity results. Moreover, yellow and red bricks had the lowest thermal conductivity (0.95 and 1.03 W. m^{-1}. K^{-1}), followed by glass aggregates (1.19 W. m^{-1}. K^{-1}). Similarly, aged and new HMA and concrete aggregates had higher thermal conductivity, 1.65, 1.91, and 2.45 W. m^{-1}. K^{-1}. The reason is similarly attributed to the different densities of clay bricks, chemical compositions, and molecular structure of glass and concrete. Therefore, concrete aggregates, as conductive materials, transfer the absorbed heat to the asphalt mixture and base course, providing a cooler surface and less thermal gradient between the surface and the environment during the day. However, bleeding and raveling (aggregate loss) are the most common chip seal deteriorations. These deteriorations stem from some reasons, including aggregate abrasion, traffic loads, and hot weather. Also, the bitumen stiffness is reduced in hot weather, resulting in aggregate movement and less aggregate-bitumen adhesion [95,96]. Thus, if the thermal conductivity of chip seal aggregates is lower, such as clay bricks and glass, less heat is transferred to the underneath bitumen which prevents chip seal degradation in hot seasons. Besides, the specific heat capacity of CDW materials, aged, and new HMA was calculated with Eq. 8 [80].Where e represents the thermal effusivity (W. $s^{1/2}$. m^{-2}. K^{-1}), k is the thermal conductivity (W. m^{-1}. K^{-1}), ρ is the material's density (kg.m^{-3}), and C_p is the specific heat capacity (J. kg^{-1}. K^{-1}). The specific heat capacity is the amount of heat (J) that can increase the one-unit weight of the material's temperature by 1 ℃ (Mirzanamadi et al., 2018). If the surface materials have higher C_p, more heat energy is required to increase the surface temperature by 1 ℃. However, the specific heat capacity changes at different temperatures, and different results may be achieved if this parameter is chosen as an influential factor on the UHI. For instance, increasing temperatures can increase the specific heat capacity of most crystalline solids, such as concrete [97]. In this study, thermal parameters were measured at room temperature (around 24 ℃), and the specific heat capacity of different materials and mixtures had little differences, ranging from 729.74 to 967.61 J. kg^{-1}. K^{-1} for glass and red brick aggregates, respectively. Another thermal parameter, which was calculated from the experimental data, is thermal diffusivity. This parameter shows how fast the absorbed heat spreads in the material. As a result, using a material with high thermal diffusivity increases the internal temperature [98]. The thermal diffusivity was calculated with Eq. 9 [80].

$$\alpha = \frac{k}{C_p \rho} \tag{9}$$

Where α represents the thermal diffusivity ($m^2.s^{-1}$), k is the thermal conductivity (W. m^{-1}. K^{-1}), C_p is the specific heat capacity (J. kg^{-1}. K^{-1}) and ρ is the density of the material (kg.m^{-3}). Thermal diffusivity has a direct relationship with thermal conductivity [80]. Regarding Table 5, the values of thermal diffusivity follow the same order as thermal conductivity. Indeed, clay bricks and glass aggregates had the lowest thermal diffusivity, 0.56 and 0.66 $mm^2.s^{-1}$, and concrete aggregates' thermal diffusivity was more than double (1.29 $mm^2.s^{-1}$) of these materials. These values are also attributed to the chemical composition, molecular structure, and density of these materials [93,94]. Although higher thermal diffusivity of asphalt mixture cools down the surface of asphalt pavement which is desirable for UHI alleviation [99], it can increase the temperature of chip seal's bitumen, contributing to bleeding and raveling deterioration in hot seasons, and the effect of albedo should not be neglected. Finally, all measured and calculated values of thermal parameters in this section were comparable with previous studies in which similar materials were investigated [100–105].

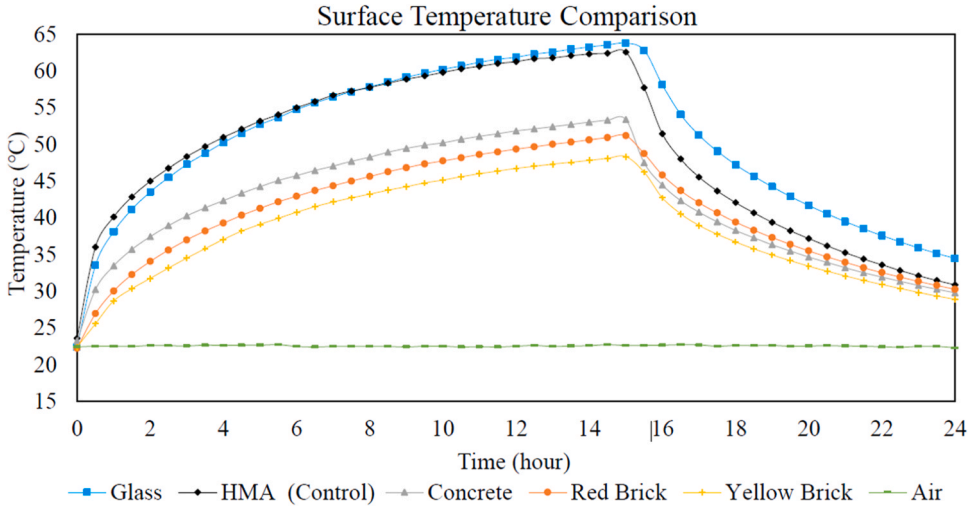

Fig. 14. The comparison of the chip seals' surface temperatures.

4.3. The Indoor Cooling Effect Evaluation

The indoor solar simulation tests revealed the surface and in-depth temperatures of chip seals and HMA. The comparison of surface temperatures of different chip seals and HMA is illustrated in Fig. 14. Regarding this Figure, the surface temperature of HMA coated with the yellow brick chip seal after 15 hours of exposure to the tungsten infrared lamp was the coolest, around 48 ℃, which was 23 % lower than the HMA without chip seals (almost 63 ℃). The second and third cooler surfaces were red brick and concrete chip seals, 18 % and 15 % lower than the HMA. The cooler surfaces of these chip seals are attributed to their lighter colors and higher VIS/NIR reflectivity which was explained in Section 4.1. Hence, these chip seals absorbed less heat, resulting in lower surface temperatures. This was also observed in previous studies about reflective coatings which reduced the asphalt pavement temperature [85–87]. In contrast, although the surface temperature of the glass chip seal was a little lower than the HMA in the first 7 hours, it reached a peak of 63.79 ℃ after 15 hours of heating with the lamp. The reason is related to the transparency of glass aggregates through which the light passes and the black color of bitumen absorbs the light, increasing the chip seal temperature. Besides, glass aggregates have a low thermal diffusivity and conductivity, tending to keep the heat rather than transferring it to the layers below.

When the tungsten lamp was turned off (night simulation), the specimens released their heat to the environment from their surfaces since they were insulated with liquid foams. As can be seen in Fig. 14, the concrete chip seal lost its heat much faster than other chip seals and its temperature was even lower than the red brick. In the first hours, this temperature reduction was faster due to the high thermal gradient between the chip seal and air temperature. However, yellow brick, red brick, and glass chip seals reduced their temperatures slowly. These different heat release rates are attributed to the thermal conductivity and thermal effusivity of chip seal aggregates which was reported in Table 5. Therefore, clay bricks and glass aggregates tend to keep the heat rather than release the heat, and concrete aggregates and the HMA tend to release heat faster to reach the thermal equilibrium with their surroundings. Therefore, the HMA and concrete chip seals released more absorbed heat at night. This night heat release of conductive materials was also observed in previous studies [27]. However, the heat absorption and heat release of the concrete chip seal was much less than the HMA due to its higher reflectivity. As the specific heat capacity of chip seal aggregates at the same temperature was in a similar range (Table 4) and the heat exchange has a direct relationship with the temperature change [80], the more temperature reduction is observed in the specimen, the more heat is released by the specimen to its surroundings. Considering Fig. 14, yellow and red brick chip seals had the lowest temperature change after the 7 hours in the ambient temperature, 40 % and 41 %, followed by concrete (44 %) and glass (46 %) chip seals. Although the thermal conductivity and effusivity of glass aggregates were lower than concrete aggregates, this higher temperature change is attributed to its higher thermal gradient with the ambient air, around 41 ℃, in comparison to the concrete chip seal's thermal gradient (30 ℃). The highest heat release was also related to the HMA due to the 51 % temperature reduction.

In addition to the surface temperature, the 25 mm-depth temperatures of chip seals and HMA during 24 hours are demonstrated in Fig. 15. As the trends of temperature change in different depths of HMA coated with chip seal and uncoated HMA were similar and only the temperature values were different, only 25 mm-depth temperatures are discussed. As can be seen, the temperature values' order for different chip seals is similar to the surface temperature comparison. However, there are some slight differences. Compared to surface temperatures, the 25 mm-depth temperatures of yellow and red bricks were much lower than the concrete chip seal after 15 hours of heating. This difference is because of the lower thermal conductivity and diffusivity of clay brick which acts as an insulation layer at the top of the HMA, transferring less heat to the HMA. Besides, the 25 mm-depth temperature of the glass chip seal was almost equal to the HMA after 15 hours. This means that less heat penetrated the HMA coated with this chip seal due to the lower thermal conductivity and diffusivity of glass aggregates. These results were comparable with previous research in which insulation and conductive materials were used as HMA materials [106,107].

4.4. The Outdoor Cooling Effect and Albedo Assessment

The albedo of six different areas, including yellow brick, red brick, concrete, and glass, new and aged HMA was measured and recorded 3 times in 3 subsequent hours as explained in Section 3.5. The average of albedo, incident, and reflected solar radiation for these six areas is reported in Fig. 16. Regarding the error bars for these parameters, the measurements had negligible differences. As is seen, the trend of albedo is similar to the UV–VIS–NIR spectrometer results. So, the yellow brick chip seal had the highest albedo, 0.24, which was approximately 2 and 6 times more than the aged and new HMA respectively. Similarly, the second and third highest albedo were related to the red brick chip seal and concrete chip seal, 0.22 and 0.21, respectively. However, the glass chip seal and new HMA repeatedly had the lowest albedo, both around 0.05. The higher albedo of clay brick and concrete chip seals is attributed to the lighter color and chemical composition of aggregates, and the low albedo of glass chip seal and HMA is because of their dark colors which absorb most solar wavelengths. The higher albedo of aged HMA, in comparison to new HMA, is related to its lighter color due to weathering, stemming from the chemical reaction of asphaltene after solar and other environmental factors exposure [36]. These results were consistent with the previous findings related to the construction materials and coatings albedo [78,108]. Pavement's albedo plays a significant role in heat output. As Chen et al. (2017) proved, pavements with higher albedo release more heat during the day (due to higher reflectivity) and less heat at night, which can alleviate the UHI effects. The reflected radiation has a marginal effect on the overall heat release during the day if there are not many high-rise buildings around the pavement [12]. Accordingly, clay bricks and concrete chip seals can mitigate the UHI dramatically due to their higher albedo.

The surface and 25 mm-depth temperatures of chip seals, aged and new HMA at the end of the albedo test, when all areas reached their maximum temperatures, are depicted in Fig. 17. As is seen, the results were similar to the indoor tungsten lamp test. Indeed, the yellow brick had the coolest surface and in-depth temperatures, 25.1 ℃ and 21.2 ℃. Compared to the aged and new HMA, the yellow

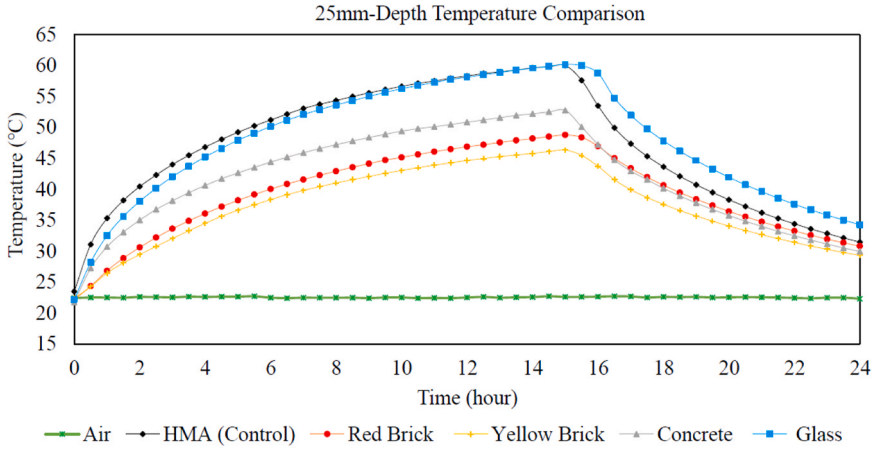

Fig. 15. The comparison of the chip seals' 25 mm-depth temperatures.

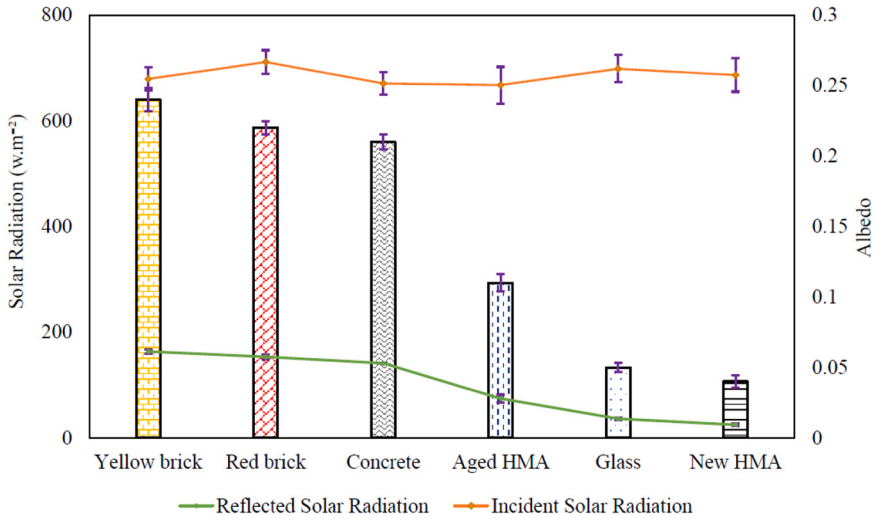

Fig. 16. The average of albedo, incident, and reflected solar radiation.

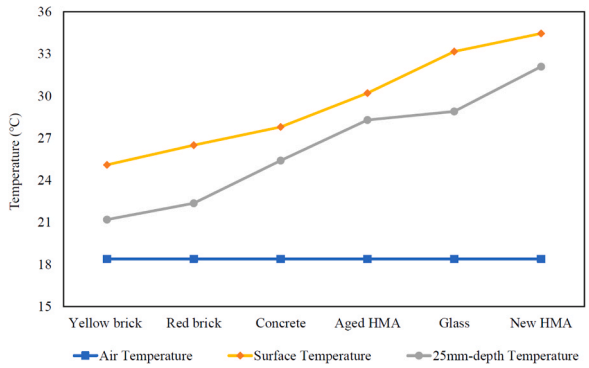

Fig. 17. The surface and 25 mm-depth temperatures of chip seals, aged and new HMA.

brick had 17 % and 27 % cooler surface respectively. Similarly, red brick and concrete had the second and third cooler surface and in-depth temperatures, 23 %, and 19 % lower surface temperatures compared with the new HMA. The glass chip seal surface temperature, however, was 3 ℃ higher than the aged HMA, and it was almost the same as the new HMA. The cooler surface and in-depth

temperatures of clay bricks and concrete, and higher temperatures of glass are attributed to their albedo. This means that higher albedo brings about lower surface and in-depth temperature which was comparable with previous studies [12]. Besides, clay bricks and glass chip seals decreased the in-depth temperatures effectively due to the lower thermal conductivity and thermal diffusivity of their aggregates.

4.5. Model Validation

Since the pavement's temperature is usually higher than the air temperature at night in summer, the CFD simulation was performed for the nighttime (9 hours), based on the indoor solar simulation test, to evaluate the UHI effects. As yellow brick and concrete chip seals showed suitable performance in terms of UHI mitigation, HMA covered with yellow brick and concrete chip seals and control HMA were compared in terms of heat release and increasing the air temperature at night. A vertical plane in the center of each model was chosen to determine the temperature difference in the pavement's depths and air, as demonstrated in Fig. 18.

The surface and 25 mm-depth temperatures of yellow brick chip seals and HMA, obtained from the laboratory tests and developed models, were compared to verify the numerical results. This comparison is illustrated in Fig. 19. Considering these results, the data obtained from the laboratory test and modeling had marginal differences, indicating the high precision of the model. For example, the HMA surface temperature achieved from the experiment had only around 1–3 ℃ differences. Similar precision was observed for surface and in-depth temperatures during the 9-hour nighttime heat release, and the temperature difference was always less than 3℃. Therefore, this model can be used to investigate the effect of the developed chip seal on the air temperature reduction as this parameter was difficult to measure with experimental methods.

4.6. The Nighttime Heat Release Simulation

After finishing the 9-hour nighttime simulation, yellow brick and concrete chip seals and HMA temperature contours were obtained, and the yellow brick and HMA temperatures are depicted in Fig. 20. As the inlet and outlet air temperatures of the models were assumed to be constant, the most heat exchange occurred at the top of the pavements where the highest temperature gradients were observed. Regarding this figure, the pavement and its surroundings' air temperatures were lower than the HMA. This lower pavement temperature after using chip seals was also observed in the laboratory and field test, which is attributed to the higher reflectivity of bricks, reducing the heat absorption during the day. It was concluded that when a lower surface temperature is available, less heat release occurs due to the lower thermal gradient between the pavement and air. Although at the beginning of the nighttime, the yellow brick chip seal and HMA surface temperatures had a large difference, 14 ℃, they had a marginal difference after 9 hours of heat release, showing much higher heat output of HMA.

Measuring the air temperature variation at the top of pavements with experimental tests would be challenging due to some parameters such as airflow and control chamber complexity. Thus, air temperature increase due to the heat release of pavements was evaluated using CFD simulation, depicted in Fig. 21. Additionally, with the boundary condition and simulation assumptions, the air temperature in the model was assumed to be 22.60 ℃, which was the same temperature as inlet and outlet air. Moreover, considering the huge dimensions of the models and wind velocity based on the input expression, only air temperature up to a height of 55 cm was increased due to the pavements' heat release at night. As the same wind velocity and airflow were assumed for yellow brick and concrete chip seals and HMA models, using yellow brick and concrete chip seal reduced the surrounding air temperature from 33 ℃ to

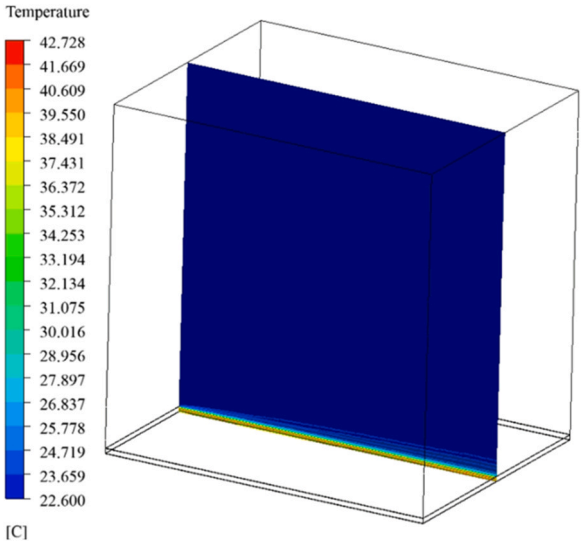

Fig. 18. The vertical plane position in the models for temperature determination.

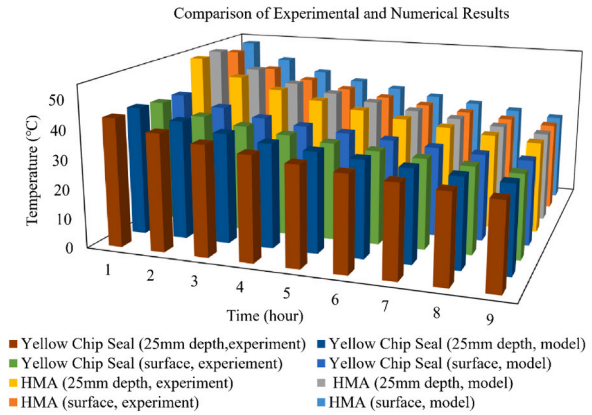

Fig. 19. The experimental and numerical temperature data comparison.

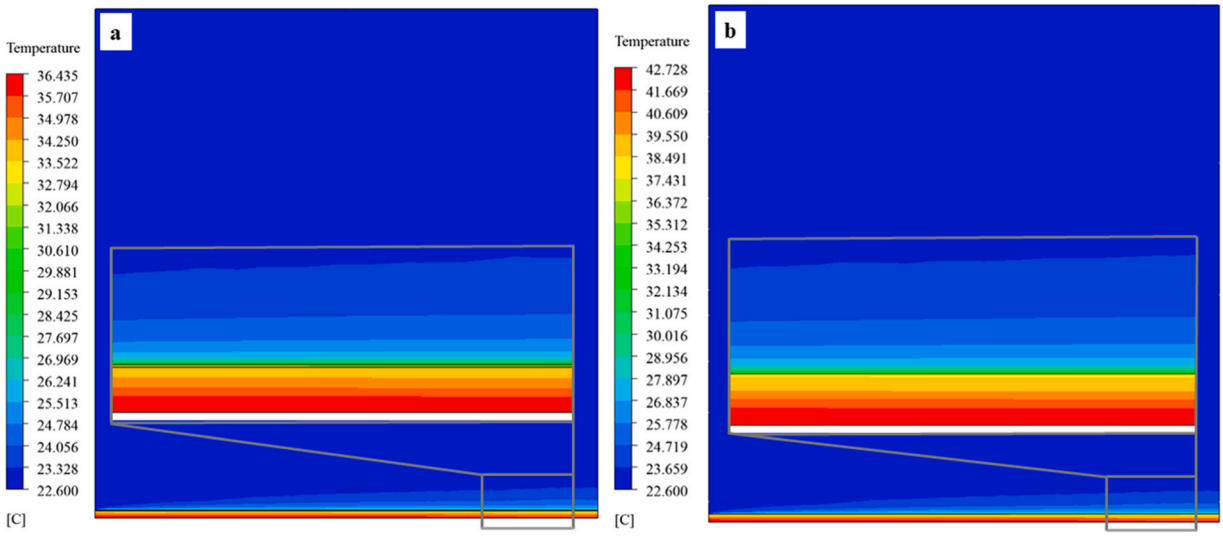

Fig. 20. The (a) yellow chip seal and (b) HMA temperature contours after 9 hours of heat release.

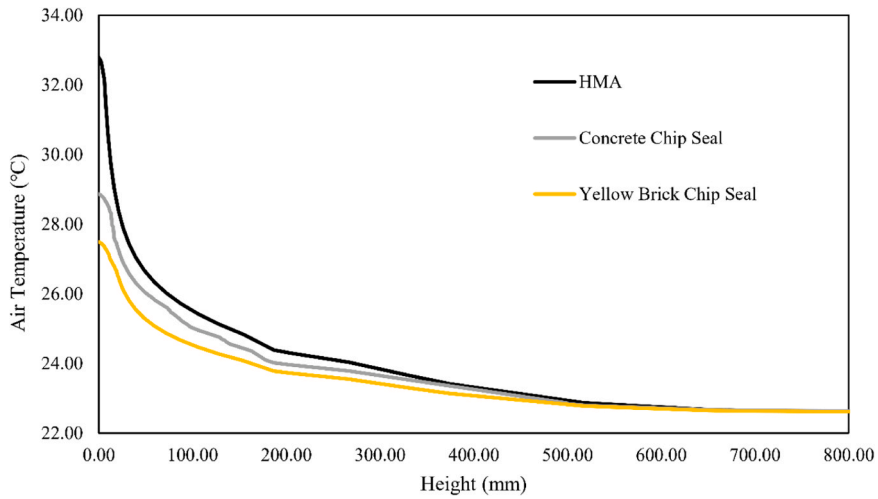

Fig. 21. The yellow brick and concrete chip seals and HMA's surrounding air temperature variation at heights.

27 ℃ and 28.5 ℃ respectively. Increasing the height, however, reduced this air temperature difference due to higher wind velocity, huge model dimensions, and constant inlet and outlet air temperature assumption. Therefore, as the air temperature is not constant at different heights in actual situations, the air temperature reduction at higher altitudes cannot be achieved with the model's assumptions. The results of the CFD simulation revealed that using clay brick and concrete chip seals can also decrease the pavement's surrounding air temperature effectively.

5. Conclusion

The dark surface of asphalt pavements is reported to cause a serious environmental issue for cities called urban heat islands (UHI). Besides, construction and demolition waste (CDW) generations have been increasing due to urbanization and population growth all over the world. Accordingly, this study offers a novel approach to not only recycle high quantities of these materials with low costs but also reduce the negative impact of asphalt pavements on the UHI effects. For these purposes, yellow and red clay bricks, concrete, and glass were used as chip seals' aggregates to increase the pavement reflectivity and decrease its temperature and heat emissions.

Regarding the laboratory tests, UV-Visible-NIR spectrometer results indicated that the solar reflectance of yellow brick, red brick, and concrete chip seals was approximately 2.5, 2, and 1.8 times higher than aged HMA. This higher reflectivity was attributed to the chemical composition and lighter color of these materials. The solar simulation test depicted that the surface temperatures of yellow brick, red brick, and concrete chip seals were 23 %, 18 %, and 15 % lower than the HMA surface, respectively. As the surface temperature change can be a good indicator of heat release into the environment, the clay bricks and concrete chip seals had the lowest temperature changes. This means that these materials absorbed less energy due to their higher reflectivity during the day, and clay brick chip seals emitted even less heat to the environment at night because of their lower thermal effusivity.

Turning to the field test results, albedo, which represents the surface reflectivity, revealed similar results. The yellow brick albedo was about 2 and 6 times more than the aged and new HMA, followed by red brick and concrete. This lower albedo reduced both surface and in-depth temperatures. As a result, the surface temperature of the yellow brick was 27 % and 17 % cooler than the new and aged HMA. Since higher albedo can decrease the surface and in-depth temperatures, the clay brick and concrete chip seals release less heat at night, which can alleviate the UHI effects dramatically. Furthermore, some numerical models revealed beneficial results regarding the air temperature reduction at night. Assuming constant air temperature in the height and summer wind conditions, the results revealed that using clay brick and concrete chip seals decreased the air temperature at least by 18 % and 14 % respectively, alleviating the UHI effects successfully.

Overall, the numerical modeling, laboratory, and field tests revealed similar trends, indicating the benefits of using clay bricks and concrete aggregates for chip seal preparation, which can mitigate the UHI and reduce cities' temperatures effectively. One important advantage of using these chip seals is that they can even increase the skid resistance which is the weakness of similar reflective pavement methods based on reflective coatings. The other environmental benefit is recycling these waste materials and decreasing the demand for virgin materials. According to the test results, glass chip seals could not reduce the HMA and air temperature due to high solar radiation absorption. Therefore, glass aggregates are not recommended for chip seal preparation as a UHI mitigation approach. Finally, as the mechanical properties, safety, and durability of concrete and brick chip seals were tested in another study [25], the suitable chip seal aggregate can be chosen based on the traffic volume of the road.

CRediT authorship contribution statement

Mohsen Shamsaei: Writing – original draft, Visualization, Validation, Software, Resources, Methodology, Investigation, Formal analysis, Data curation, Conceptualization. **Michel Vaillancourt:** Writing – review & editing, Validation, Supervision, Resources, Project administration, Funding acquisition, Conceptualization. **Alan Carter:** Writing – review & editing, Validation, Supervision, Project administration, Funding acquisition, Conceptualization.

Declaration of Competing Interest

The authors declare that they have no known competing financial interests or personal relationships that could have appeared to influence the work reported in this paper.

Data Availability

Data will be made available on request.

Acknowledgments

The Natural Sciences and Engineering Research Council of Canada (NSERC) is acknowledged for the financial assistance [funding reference number: RGPIN-2020-04861]. We would also acknowledge the laboratory assistance of Sylvain Bibeau, Francis Bilodeau, Richard Prowt, and Sébastien Ménard.

References

[1] Y. Qin, J.E. Hiller, Understanding pavement-surface energy balance and its implications on cool pavement development, Energy Build. 85 (2014) 389–399, https://doi.org/10.1016/j.enbuild.2014.09.076.
[2] M. Shamsaei, A. Carter, M. Vaillancourt, A review on the heat transfer in asphalt pavements and urban heat island mitigation methods, Constr. Build. Mater. 359 (2022) 129350, https://doi.org/10.1016/j.conbuildmat.2022.129350.
[3] M. Santamouris, Energy and Climate in the Urban Built Environment (ed), Routledge, London, 2013, https://doi.org/10.4324/9781315073774.
[4] H. Akbari, L.S. Rose, Urban surfaces and heat island mitigation potentials, J. Hum. -Environ. Syst. 11 (2008) 85–101.
[5] P.E. Phelan, K. Kaloush, M. Miner, J. Golden, B. Phelan, H. Silva, R.A. Taylor, Urban Heat Island: Mechanisms, Implications, and Possible Remedies, Annu. Rev. Environ. Resour. 40 (2015) 285–307, https://doi.org/10.1146/annurev-environ-102014-021155.
[6] C. Sarrat, A. Lemonsu, V. Masson, D. Guedalia, Impact of urban heat island on regional atmospheric pollution, Atmos. Environ. 40 (2006) 1743–1758, https://doi.org/10.1016/j.atmosenv.2005.11.037.
[7] M. Kolokotroni, X. Ren, M. Davies, A. Mavrogianni, London's urban heat island: Impact on current and future energy consumption in office buildings, Energy Build. 47 (2012) 302–311, https://doi.org/10.1016/j.enbuild.2011.12.019.
[8] G.B. Anderson, M.L. Bell, Heat Waves in the United States: Mortality Risk during Heat Waves and Effect Modification by Heat Wave Characteristics in 43 U.S. Communities, Environ. Health Perspect. 119 (2011) 210–218, https://doi.org/10.1289/ehp.1002313.
[9] J. Yang, L. Hu, C. Wang, Population dynamics modify urban residents' exposure to extreme temperatures across the United States, Sci. Adv. 5 (2019) eaay3452, https://doi.org/10.1126/sciadv.aay3452.
[10] A. Sha, Z. Liu, K. Tang, P. Li, Solar heating reflective coating layer (SHRCL) to cool the asphalt pavement surface, Constr. Build. Mater. 139 (2017) 355–364, https://doi.org/10.1016/j.conbuildmat.2017.02.087.
[11] H.R. Silva, P.E. Phelan, J.S. Golden, Modeling effects of urban heat island mitigation strategies on heat-related morbidity: a case study for Phoenix, Arizona, USA, Int. J. Biometeorol. 54 (2010) 13–22, https://doi.org/10.1007/s00484-009-0247-y.
[12] J. Chen, H. Wang, H. Zhu, Analytical approach for evaluating temperature field of thermal modified asphalt pavement and urban heat island effect, Appl. Therm. Eng. 113 (2017) 739–748, https://doi.org/10.1016/j.applthermaleng.2016.11.080.
[13] C. Zhang, M. Hu, F. Di Maio, B. Sprecher, X. Yang, A. Tukker, An overview of the waste hierarchy framework for analyzing the circularity in construction and demolition waste management in Europe, Sci. Total Environ. 803 (2022) 149892, https://doi.org/10.1016/j.scitotenv.2021.149892.
[14] B. Huang, X. Wang, H. Kua, Y. Geng, R. Bleischwitz, J. Ren, Construction and demolition waste management in China through the 3R principle, Resour. Conserv. Recycl. 129 (2018) 36–44, https://doi.org/10.1016/j.resconrec.2017.09.029.
[15] S. Shooshtarian, T. Maqsood, S. Caldera, T. Ryley, Transformation towards a circular economy in the Australian construction and demolition waste management system, Sustain. Prod. Consum. 30 (2022) 89–106, https://doi.org/10.1016/j.spc.2021.11.032.
[16] M. Yeheyis, K. Hewage, M.S. Alam, C. Eskicioglu, R. Sadiq, An overview of construction and demolition waste management in Canada: a lifecycle analysis approach to sustainability, Clean. Technol. Environ. Policy 15 (2013) 81–91, https://doi.org/10.1007/s10098-012-0481-6.
[17] A.S. Molla, P. Tang, W. Sher, D.N. Bekele, Chemicals of concern in construction and demolition waste fine residues: A systematic literature review, J. Environ. Manag. 299 (2021) 113654, https://doi.org/10.1016/j.jenvman.2021.113654.
[18] M. Menegaki, D. Damigos, A review on current situation and challenges of construction and demolition waste management, Curr. Opin. Green. Sustain. Chem. 13 (2018) 8–15, https://doi.org/10.1016/j.cogsc.2018.02.010.
[19] U.A. Umar, N. Shafiq, A. Malakahmad, M.F. Nuruddin, M.F. Khamidi, A review on adoption of novel techniques in construction waste management and policy, J. Mater. Cycles Waste Manag. 19 (2017) 1361–1373, https://doi.org/10.1007/s10163-016-0534-8.
[20] S. Ulubeyli, A. Kazaz, V. Arslan, Construction and Demolition Waste Recycling Plants Revisited: Management Issues, Procedia Eng. 172 (2017) 1190–1197, https://doi.org/10.1016/j.proeng.2017.02.139.
[21] R. Khafajeh, M. Shamsaei, A. Latifi, B. Amin Javaheri, M. Vaillancourt, Comprehensive Investigation of Influential Mix-Design Factors on the Microsurfacing Mixture Performance, J. Mater. Civ. Eng. 35 (2023) 04023214, https://doi.org/10.1061/JMCEE7.MTENG-15212.
[22] P.A. Serigos, A. de F. Smit, J.A. Prozzi, University of Texas at Austin. Center for Transportation Research, Performance of preventive maintenance treatments for flexible pavements in Texas., 2017. https://rosap.ntl.bts.gov/view/dot/32140 (accessed January 26, 2023).
[23] M.A. Montoya, W. Jason Weiss, J.E. Haddock, Using electrical resistance to evaluate the chip seal curing process, Road. Mater. Pavement Des. 18 (2017) 98–111, https://doi.org/10.1080/14680629.2017.1389090.
[24] L. You, Z. You, Q. Dai, X. Xie, S. Washko, J. Gao, Investigation of adhesion and interface bond strength for pavements underlying chip-seal: Effect of asphalt-aggregate combinations and freeze-thaw cycles on chip-seal, Constr. Build. Mater. 203 (2019) 322–330, https://doi.org/10.1016/j.conbuildmat.2019.01.058.
[25] M. Shamsaei, A. Carter, M. Vaillancourt, Using Construction and Demolition Waste Materials to Develop Chip Seals for Pavements, Infrastructures 8 (2023) 95, https://doi.org/10.3390/infrastructures8050095.
[26] M. Shamsaei, A. Carter, M. Vaillancourt, The Comparison of the Bleeding Potential of Chip Seals Developed with Recycled Materials and Limestone Aggregates, in: Springer Nature Switzerland, Cham, 2024, pp. 521–531.
[27] A. Mohajerani, J. Bakaric, T. Jeffrey-Bailey, The urban heat island effect, its causes, and mitigation, with reference to the thermal properties of asphalt concrete, J. Environ. Manag. 197 (2017) 522–538, https://doi.org/10.1016/j.jenvman.2017.03.095.
[28] C. Richard, G. Doré, C. Lemieux, J.-P. Bilodeau, J. Haure-Touzé, Albedo of Pavement Surfacing Materials: In Situ Measurements, (2015) 181–192. https://doi.org/10.1061/9780784479315.017.
[29] N. Xie, H. Li, A. Abdelhady, J. Harvey, Laboratorial investigation on optical and thermal properties of cool pavement nano-coatings for urban heat island mitigation, Build. Environ. 147 (2019) 231–240, https://doi.org/10.1016/j.buildenv.2018.10.017.
[30] M. Zheng, Y. Tian, L. He, Analysis on Environmental Thermal Effect of Functionally Graded Nanocomposite Heat Reflective Coatings for Asphalt Pavement, Coatings 9 (2019) 178, https://doi.org/10.3390/coatings9030178.
[31] Y. Lu, M.A. Rahman, N.W. Moore, A.J. Golrokh, Lab-Controlled Experimental Evaluation of Heat-Reflective Coatings by Increasing Surface Albedo for Cool Pavements in Urban Areas, Coatings 12 (2022) 7, https://doi.org/10.3390/coatings12010007.
[32] Y. Chen, Z. Li, S. Ding, X. Yang, T. Guo, Research on heat reflective coating technology of asphalt pavement, Int. J. Pavement Eng. 23 (2022) 4455–4464, https://doi.org/10.1080/10298436.2021.1952410.
[33] V.D. Maria, M. Rahman, P. Collins, G. Dondi, C. Sangiorgi, Urban Heat Island Effect: Thermal Response from Different Types of Exposed Paved Surfaces, Int. J. Pavement Res. Technol. 6 (2013) 414–422, https://doi.org/10.6135/ijprt.org.tw/2013.6(4).414.
[34] M. Nishioka, M. Nabeshima, S. Wakama, J. Ueda, Effects of surface temperature reduction and thermal environment on high albedo coating asphalt pavement, J. Heat. Isl. Inst. Int 1 (2006) 46–52.
[35] M. Zheng, L. Han, F. Wang, H. Mi, Y. Li, L. He, Comparison and analysis on heat reflective coating for asphalt pavement based on cooling effect and anti-skid performance, Constr. Build. Mater. 93 (2015) 1197–1205, https://doi.org/10.1016/j.conbuildmat.2015.04.043.
[36] N. Xie, H. Li, H. Zhang, X. Zhang, M. Jia, Effects of accelerated weathering on the optical characteristics of reflective coatings for cool pavement, Sol. Energy Mater. Sol. Cells 215 (2020) 110698, https://doi.org/10.1016/j.solmat.2020.110698.
[37] M. Shamsaei, I. Aghayan, K.A. Kazemi, Experimental investigation of using cross-linked polyethylene waste as aggregate in roller compacted concrete pavement, J. Clean. Prod. 165 (2017) 290–297, https://doi.org/10.1016/j.jclepro.2017.07.109.
[38] M. Shamsaei, R. Khafajeh, I. Aghayan, Laboratory evaluation of the mechanical properties of roller compacted concrete pavement containing ceramic and coal waste powders, Clean. Technol. Environ. Policy 21 (2019) 707–716, https://doi.org/10.1007/s10098-018-1657-5.
[39] M. Shamsaei, R. Khafajeh, H. Ghasemzadeh Tehrani, I. Aghayan, Experimental evaluation of ceramic waste as filler in hot mix asphalt, Clean. Technol. Environ. Policy 22 (2020) 535–543, https://doi.org/10.1007/s10098-019-01788-9.

[40] I. Aghayan, R. Khafajeh, M. Shamsaei, Life cycle assessment, mechanical properties, and durability of roller compacted concrete pavement containing recycled waste materials, Int. J. Pavement Res. Technol. 14 (2021) 595–606, https://doi.org/10.1007/s42947-020-0217-7.
[41] A. Mammeri, M. Lallam, S.E. Guellati, M. Shamsaei, Using Tuff and Limestone Sand to Minimize Water Consumption of Pavement Construction in Arid Regions, Civ. Environ. Eng. 19 (2023) 630–639, https://doi.org/10.2478/cee-2023-0057.
[42] M. Contreras Llanes, M. Romero Pérez, M.J. Gázquez González, J.P. Bolívar Raya, Construction and demolition waste as recycled aggregate for environmentally friendly concrete paving, Environ. Sci. Pollut. Res. 29 (2022) 9826–9840, https://doi.org/10.1007/s11356-021-15849-4.
[43] A.R. Pasandín, I. Pérez, Laboratory evaluation of hot-mix asphalt containing construction and demolition waste, Constr. Build. Mater. 43 (2013) 497–505, https://doi.org/10.1016/j.conbuildmat.2013.02.052.
[44] R. Khafajeh, M. Shamsaei, H.G. Tehrani, S.M. Easa, Proposing Load Transfer Efficiency as Criterion for Repairing Longitudinal and Transverse Cracks of Asphalt Pavements, J. Transp. Eng. Part B Pavements 147 (2021) 06021002, https://doi.org/10.1061/JPEODX.0000301.
[45] R. Khafajeh, M. Shamsaei, M. Irvani, H. Ezati, M. Vaillancourt, The Development of a Finite Element Model for the Estimation of Load Transfer Efficiency in Transverse Cracks of Asphalt Pavement, Int. J. Pavement Res. Technol. (2023), https://doi.org/10.1007/s42947-023-00334-7.
[46] P. Deb, Kh.L. Singh, Experimental Investigation on the Mechanical Performance of Cold Mix Asphalt Using Construction Demolition Waste as Filler, Int. J. Pavement Res. Technol. (2022), https://doi.org/10.1007/s42947-022-00216-4.
[47] A. M. Arisha, A.R. Gabr, S.M. El-Badawy, S.A. Shwally, Performance Evaluation of Construction and Demolition Waste Materials for Pavement Construction in Egypt, J. Mater. Civ. Eng. 30 (2018) 04017270, https://doi.org/10.1061/(ASCE)MT.1943-5533.0002127.
[48] É. Lachance-Tremblay, M. Vaillancourt, D. Perraton, Evaluation of the impact of recycled glass on asphalt mixture performances, Road. Mater. Pavement Des. 17 (2016) 600–618, https://doi.org/10.1080/14680629.2015.1103778.
[49] S. Mohsenian Hadad Amlashi, M. Vaillancourt, A. Carter, J.-P. Bilodeau, Resilient modulus of pavement unbound granular materials containing recycled glass aggregate, Mater. Struct. 51 (2018) 89, https://doi.org/10.1617/s11527-018-1219-7.
[50] L. Moretti, G. Cantisani, M. Carpiceci, A. D'Andrea, G. Del Serrone, P. Di Mascio, P. Peluso, G. Loprencipe, Investigation of Parking Lot Pavements to Counteract Urban Heat Islands, Sustainability 14 (2022) 7273, https://doi.org/10.3390/su14127273.
[51] A.A. Gheni, O.I. Abdelkarim, M.M. Abdulazeez, M.A. ElGawady, Texture and design of green chip seal using recycled crumb rubber aggregate, J. Clean. Prod. 166 (2017) 1084–1101, https://doi.org/10.1016/j.jclepro.2017.08.127.
[52] A. Durrani, Analysis of Reclaimed Asphalt Pavement (RAP) Proposed for Use as Aggregate in Microsurfacing and Chip Seal Mixes for Local Roadways Applications in Ohio, Ohio University, 2021. https://etd.ohiolink.edu/apexprod/rws_olink/r/1501/10?clear=10&p10_accession_num=ohiou1628337066238648 (accessed January 28, 2023).
[53] C. Liu, D. Yuan, Temperature Distribution in Layered Road Structures, J. Transp. Eng. 126 (2000) 93–95, https://doi.org/10.1061/(ASCE)0733-947X(2000)126:1(93).
[54] I. Adwan, A. Milad, Z.A. Memon, I. Widyatmoko, N. Ahmat Zanuri, N.A. Memon, N.I.M. Yusoff, Asphalt Pavement Temperature Prediction Models: A Review, Appl. Sci. 11 (2021) 3794, https://doi.org/10.3390/app11093794.
[55] ASTM C127, Standard test method for relative density (specific gravity) and absorption of coarse aggregate, Am. Soc. Test. Mater. West Conshohocken PA USA (2015).
[56] ASTM C29/C29M, Standard Test Method for Bulk Density ("Unit Weight") and Voids in Aggregate, American Society for Testing and Materials, West Conshohocken, PA, USA, 2017.
[57] ASTM C131/C131M, Standard test method for resistance to. degradation of small-size coarse aggregate by abrasion and impact in the Los Angeles machine, Am. Soc. Test. Mater. West, Conshohocken PA USA, 2020.
[58] ASTM D4791, Standard test method for flat particles, elongated particles, or flat and elongated particles in coarse aggregate, American Society for Testing and Materials, West Conshohocken, PA, USA, 2019.
[59] ASTM C136/C136M, Standard Test Method for Sieve Analysis of Fine and Coarse Aggregates, in: American Society for Testing and Materials, West Conshohocken, PA, USA, 2019.
[60] ASTM D6997, Standard Test Method for Distillation of Emulsified Asphalt., American Society for Testing and Materials, West Conshohocken, PA, USA, 2020.
[61] ASTM D6936, Standard Test Method for Determining Demulsibility of Emulsified Asphalt, Am. Soc. Test. Mater. West Conshohocken PA USA (2017).
[62] ASTM D7496, Standard test method for viscosity of emulsified asphalt by saybolt furol viscometer. Annual book of ASTM standards, American Society for Testing and Materials, West Conshohocken, PA, USA, 2018.
[63] ASTM D6930, Standard Test Method for Settlement and Storage Stability of Emulsified Asphalts, Am. Soc. Test. Mater. West Conshohocken PA USA (2019).
[64] ASTM D5, Standard test method for penetration of bituminous materials, Am. Soc. Test. Mater. West Conshohocken PA USA (2013).
[65] ASTM D7402, Standard Practice for Identifying Cationic Emulsified Asphalts, Am. Soc. Test. Mater. West Conshohocken PA USA (2017).
[66] ASTM D113, Standard test method for ductility of asphalt materials, Am. Soc. Test. Mater. West Conshohocken PA USA (2017).
[67] ASTM D2042, Standard test method for solubility of asphalt materials in trichloroethylene, American Society for Testing and Materials, West Conshohocken, PA, USA, 2015.
[68] N.W. McLEOD, C.W. Chaffin, A.E. Holberg, C.F. Parker, V. Obrcian, J.M. Edwards, W.H. Campen, W.J. Kari, A general method of design for seal coats and surface treatments, : Proc. Assoc. Asph. Paving Technol. (1969) 537–630.
[69] J.P. Kearby, Tests and theories on penetration surfaces, in: Highw. Res. Board Proc., 1953.
[70] W.R. Stockton, J.A. Epps, ENGINEERING ECONOMY AND ENERGY CONSIDERATIONS. SEAL COAT ECONOMICS AND DESIGN, 1975.
[71] T.J. Wood, D.W. Janisch, F.S. Gaillard, Minnesota seal coat handbook 2006, 2006.
[72] G.D. Québec, Hot mix asphalt formulated according to the Pavement Laboratory formulation method, 4 Liants Enrobés (2016) 17.
[73] ASTM D7984, Standard Test Method for Measurement of Thermal Effusivity of Fabrics Using a Modified Transient Plane Source (MTPS) Instrument, Am. Soc. Test. Mater. West, Conshohocken PA USA, 2021.
[74] B.N. Mills, S.L. Tighe, J. Andrey, J.T. Smith, K. Huen, Climate Change Implications for Flexible Pavement Design and Performance in Southern Canada, J. Transp. Eng. 135 (2009) 773–782, https://doi.org/10.1061/(ASCE)0733-947X(2009)135:10(773).
[75] L. Jiang, S. Wang, Enhancing heat release of asphalt pavement by a gradient heat conduction channel, Constr. Build. Mater. 230 (2020) 117018, https://doi.org/10.1016/j.conbuildmat.2019.117018.
[76] N. Pirouzfam, K. Sendur, Tungsten Based Spectrally Selective Absorbers with Anisotropic Rough Surface Texture, Nanomaterials 11 (2021) 2018, https://doi.org/10.3390/nano11082018.
[77] ASTM E1918, Standard Test Method for Measuring Solar Reflectance of Horizontal and Low-Sloped Surfaces in the Field, in: Am. Soc. Test. Mater. West Conshohocken PA USA, 2021.
[78] H. Li, J. Harvey, A. Kendall, Field measurement of albedo for different land cover materials and effects on thermal performance, Build. Environ. 59 (2013) 536–546, https://doi.org/10.1016/j.buildenv.2012.10.014.
[79] B. Zhou, J. Pei, B. Richard Hughes, D. SNM Nasir, B. Vital, C.A.J. Pantua, J. Calautit, J. Zhang, Structural response analysis of road pavement solar collector (RPSC) with serpentine heat pipes under validated temperature field, Constr. Build. Mater. 268 (2021) 121110, https://doi.org/10.1016/j.conbuildmat.2020.121110.
[80] T.L. Bergman, T.L. Bergman, F.P. Incropera, D.P. DeWitt, A.S. Lavine, Fundamentals of Heat and Mass Transfer, John Wiley & Sons, 2011.
[81] ASTM G173, Standard Tables for Reference Solar Spectral Irradiances: Direct Normal and Hemispherical on 37° Tilted Surface, Am. Soc. Test. Mater. West, Conshohocken PA USA, 2008.
[82] C.J. Cleveland, C. Morris, eds., Section 10 - Solar, in: Handb. Energy, Elsevier, Amsterdam, 2013: pp. 405–450. https://doi.org/10.1016/B978-0-08-046405-3.00010-3.
[83] J. Turner, A.V. Parisi, Ultraviolet Radiation Albedo and Reflectance in Review: The Influence to Ultraviolet Exposure in Occupational Settings, Int. J. Environ. Res. Public. Health 15 (2018) 1507, https://doi.org/10.3390/ijerph15071507.

[84] T. Kim, J. Uh, A Study on the Effect on UV Exposure in Coastal Buildings, J. Soc. Disaster Inf. 17 (2021) 195–205, https://doi.org/10.15683/kosdi.2021.6.30.195.
[85] A. Synnefa, M. Santamouris, K. Apostolakis, On the development, optical properties and thermal performance of cool colored coatings for the urban environment, Sol. Energy 81 (2007) 488–497, https://doi.org/10.1016/j.solener.2006.08.005.
[86] X. Cao, B. Tang, X. Zou, L. He, Analysis on the cooling effect of a heat-reflective coating for asphalt pavement, Road. Mater. Pavement Des. 16 (2015) 716–726, https://doi.org/10.1080/14680629.2015.1026383.
[87] C. Miao, Z. Li, K. Li, Y. Lv, X. Wu, X. Cao, Y. Wu, A super-cooling solar reflective coating with waterborne polyurethane for asphalt pavement, Prog. Org. Coat. 165 (2022) 106741, https://doi.org/10.1016/j.porgcoat.2022.106741.
[88] G.M. Revel, M. Martarelli, M.Á. Bengochea, A. Gozalbo, M.J. Orts, A. Gaki, M. Gregou, M. Taxiarchou, A. Bianchin, M. Emiliani, Nanobased coatings with improved NIR reflecting properties for building envelope materials: Development and natural aging effect measurement, Cem. Concr. Compos. 36 (2013) 128–135, https://doi.org/10.1016/j.cemconcomp.2012.10.002.
[89] E. Coser, V.F. Moritz, A. Krenzinger, C.A. Ferreira, Development of paints with infrared radiation reflective properties, Pol. ímeros 25 (2015) 305–310, https://doi.org/10.1590/0104-1428.1869.
[90] L. Jiang, L. Wang, S. Wang, A novel solar reflective coating with functional gradient multilayer structure for cooling asphalt pavements, Constr. Build. Mater. 210 (2019) 13–21, https://doi.org/10.1016/j.conbuildmat.2019.03.180.
[91] M. Ahmad, R.N.S. Al-Dala\'ien, S. Beddu, Z.B. Itam, Thermo-Physical Properties of Graphite Powder and Polyethylene Modified Asphalt Concrete, Eng. Sci. Volume 17 (March 2022) (2021) 121–132.
[92] J. Chen, X. Yin, H. Wang, Y. Ding, Evaluation of durability and functional performance of porous polyurethane mixture in porous pavement, J. Clean. Prod. 188 (2018) 12–19, https://doi.org/10.1016/j.jclepro.2018.03.297.
[93] P.K. Gupta, Non-crystalline solids: glasses and amorphous solids, J. Non-Cryst. Solids 195 (1996) 158–164.
[94] V.S. Ramachandran, R.F. Feldman, 1 - Concrete Science, in: V.S. Ramachandran (Ed.), Concr. Admix. Handb. Second Ed., William Andrew Publishing, Park Ridge, NJ, 1996: pp. 1–66. https://doi.org/10.1016/B978-081551373-5.50005-2.
[95] R.J. Holmgreen, J.A. Epps, C.H. Hughes, B.M. Gallaway, Field evaluation of the Texas seal coat design method, 1985.
[96] D.D. Gransberg, D.M. James, Chip seal best practices, Transportation Research Board, 2005.
[97] J. Pan, R. Zou, F. Jin, Experimental Study on Specific Heat of Concrete at High Temperatures and Its Influence on Thermal Energy Storage, Energies 10 (2017) 33, https://doi.org/10.3390/en10010033.
[98] A. Mammeri, M. Vaillancourt, M. Shamsaei, Experimental and numerical investigation of using waste glass aggregates in asphalt pavement to mitigate urban heat islands, Clean. Technol. Environ. Policy (2023), https://doi.org/10.1007/s10098-023-02481-8.
[99] Y. Chen, L. Lyu, J. Pei, G. Zhang, Y. Wen, J. Zhang, Novel Asphalt-Mix Design with High Thermal Diffusivity for Alleviating the Urban Heat Island, J. Mater. Civ. Eng. 32 (2020) 04020321, https://doi.org/10.1061/(ASCE)MT.1943-5533.0003325.
[100] M.K. Howlader, M.H. Rashid, D. Mallick, T. Haque, Effects of aggregate types on thermal properties of concrete, ARPN J. Eng. Appl. Sci. 7 (2012) 900–906.
[101] G. Kanellopoulos, V.G. Koutsomarkos, K.J. Kontoleon, K. Georgiadis-Filikas, Numerical Analysis and Modelling of Heat Transfer Processes through Perforated Clay Brick Masonry Walls, Procedia Environ. Sci. 38 (2017) 492–499, https://doi.org/10.1016/j.proenv.2017.03.112.
[102] S. Bodian, M. Faye, N.A. Sene, V. Sambou, O. Limam, A. Thiam, Thermo-mechanical behavior of unfired bricks and fired bricks made from a mixture of clay soil and laterite, J. Build. Eng. 18 (2018) 172–179, https://doi.org/10.1016/j.jobe.2018.03.014.
[103] N. Hoivik, C. Greiner, J. Barragan, A.C. Iniesta, G. Skeie, P. Bergan, P. Blanco-Rodriguez, N. Calvet, Long-term performance results of concrete-based modular thermal energy storage system, J. Energy Storage 24 (2019) 100735, https://doi.org/10.1016/j.est.2019.04.009.
[104] W.-C. Wang, H.-Y. Wang, K.-H. Chang, S.-Y. Wang, Effect of high temperature on the strength and thermal conductivity of glass fiber concrete, Constr. Build. Mater. 245 (2020) 118387, https://doi.org/10.1016/j.conbuildmat.2020.118387.
[105] J. Byzyka, M. Rahman, D.A. Chamberlain, A laboratory investigation on thermal properties of virgin and aged asphalt mixture, Constr. Build. Mater. 305 (2021) 124757, https://doi.org/10.1016/j.conbuildmat.2021.124757.
[106] D. Yinfei, S. Qin, W. Shengyue, Highly oriented heat-induced structure of asphalt pavement for reducing pavement temperature, Energy Build. 85 (2014) 23–31, https://doi.org/10.1016/j.enbuild.2014.09.035.
[107] D. Yinfei, W. Shengyue, Z. Jian, Cooling asphalt pavement by a highly oriented heat conduction structure, Energy Build. 102 (2015) 187–196, https://doi.org/10.1016/j.enbuild.2015.05.020.
[108] H. Li, N. Xie, 7 - Reflective coatings for high albedo pavement, in: F. Pacheco-Torgal, S. Amirkhanian, H. Wang, E. Schlangen (Eds.), Eco-Effic. Pavement Constr. Mater., Woodhead Publishing, 2020: pp. 127–146. https://doi.org/10.1016/B978-0-12-818981-8.00007-2.